



**University of
Zurich**^{UZH}

Spatial Variation in Soil Hydraulic Properties in the Studibach Catchment and its Effects on Simulated Infiltration

GEO 511 Master's Thesis

Author

Sonja Eisenring
18-700-310

Supervised by

Dr. Ilja van Meerveld
Tatjana Carina Speckert
Victor Gauthier

Faculty representative

Dr. Ilja van Meerveld

26.09.2023

Department of Geography, University of Zurich

Table of contents

Table of contents	1
List of figures	3
List of tables.....	4
Abbreviation.....	4
Abstract.....	5
1. Introduction	6
2. Background	8
2.1. Catena concept	8
2.2. Soil physical properties	9
2.2.1. Soil texture.....	9
2.2.2. Soil organic matter	11
2.3. Soil hydraulic properties.....	12
2.3.1. Soil water retention curves (SWRC).....	13
2.3.2. Drainable porosity	16
2.4. Hydrological models	17
3. Study site.....	20
3.1. Alptal	20
3.2. Studibach catchment.....	22
4. Methods.....	24
4.1. Field measurements.....	24
4.2. Laboratory analysis	24
4.2.1. Soil water retention and drainable porosity	24
4.2.2. Soil texture, soil organic matter, bulk density	25
4.3. Data analysis	26
4.3.1. Soil water retention curve.....	26
4.3.2. Statistical analysis	26
4.4. Model analysis	26

5. Results.....	28
5.1. Soil properties	28
5.1.1. Soil bulk density and soil resistance	28
5.1.2. Soil texture.....	29
5.1.3. Organic matter.....	30
5.2. Soil hydraulic properties.....	31
5.2.1. Water retention curves.....	31
5.2.2. Drainable porosity	36
5.3. Model simulations	36
6. Discussion	40
6.1. Spatial variation of soil hydraulic properties	40
6.1.1. Soil organic matter	40
6.1.2. Water retention and drainable porosity	40
6.2. Effect of soil hydraulic properties on hydrological response	42
6.2.1. Effect of soil hydraulic parameters	42
6.2.2. Effect of size and intensity of rainfall	43
6.2.3. Model uncertainties and the influence of subsurface lateral flow	44
7. Conclusions	45
References.....	46
Appendix.....	54
Personal declaration.....	61

List of figures

Figure 1: Illustration of soil catena.....	8
Figure 2: Soil texture triangle according to USDA classification.....	10
Figure 3: Positive correlation between SOM and TWI.....	12
Figure 4: Soil water retention curve.....	14
Figure 5: Relation of soil water retention curve to pore size distribution.....	14
Figure 6: Typical soil water retention curves with different soil texture classes.....	15
Figure 7: Soil water retention curves in grassed and forest soils.....	16
Figure 8: Relation of drainable porosity (low and high) to soil water retention curves.....	16
Figure 9: Map of the soil permeability (top 50 cm) in the Alptal.....	21
Figure 10: Map of Studibach Catchment with sub-catchments and sampling sites.....	22
Figure 11: Illustration of HYDRUS-1D model components.....	27
Figure 12: Mean soil resistance as a function of depth below the surface.....	29
Figure 13: Soil texture of the measured samples in a soil texture triangle.....	30
Figure 14: Box plots of soil organic matter at both soil depths and the relations between soil organic matter and TWI and slope.....	31
Figure 15: Box plots of the soil organic matter for the forest and grassland sites.....	31
Figure 16: Fitted water retention curves for both soil depths color-coded according to TWI.....	32
Figure 17: Non-fitted water retention curves for each site for both depths.....	33
Figure 18: Box plots showing the soil moisture content (water content) at saturation, field capacity ($pF=1.8$), and wilting point ($pF=4.2$) for both depths.....	34
Figure 19: Fitted water retention curves color-coded by vegetation.....	34
Figure 20: Mean and double standard deviation of fitted water retention curves for forest and grassland sites.....	35
Figure 21: Fitted parameters (n and α) from the Van Genuchten model in relation to topographic wetness index (TWI) for both soil depths.....	35
Figure 22: Box plots of the drainable porosity for the two soil depths and the relation between the drainable porosity and TWI and slope.....	36
Figure 23: Time series of the simulated soil moisture content for the large rainfall event for forest and grassland site at 0.5 cm, 5 cm, 15 cm and 25 cm below the soil surface.....	38
Figure 24: Time series of the simulated soil moisture content for the high-intensity rainfall event for forest and grassland site at 0.5 cm, 5 cm, 15 cm and 25 cm below the soil surface.....	39

List of tables

Table 1: Grain size fractions with ranges of grain sizes	9
Table 2: Main characteristics of the sampling sites in the Studibach catchment	23
Table 3: Soil bulk density for each sampling site at both depths	28

Abbreviation

DEM	Digital Elevation Model
DP	Drainable porosity
SOC	Soil organic carbon
SOM	Soil organic matter
SWRC	Soil water retention curve
TWI	Topographic wetness index

Abstract

The Alptal is characterised by high precipitation and low permeability soils, which can lead to overland flow, erosion, and flooding. To better understand soil hydraulic processes in mountainous catchments and the response of soils to heavy rainfall, it is essential to investigate the spatial variation of soil hydraulic properties. This thesis aims to answer how soil hydraulic properties vary spatially, in particular in relation to topography and vegetation, and how they affect rainfall redistribution during heavy rainfall. Therefore, this thesis investigates the effect of topographic wetness index (TWI), slope, and soil physical properties on soil hydraulic properties. Laboratory analyses included the measurement of water retention, drainable porosity and soil organic matter for 20 soil samples from two depths (2-7 and 10-15 cm). In addition, water redistribution was simulated using HYDURS-1D for two rainfall events. Water retention and drainable porosity at 2-7 cm soil depth were both correlated to TWI and affected by soil organic matter content. The model simulations showed that the observed differences in soil hydraulic properties affect the soil moisture response to heavy rainfall events, especially in the first 15 cm. This was mainly due to the variation in the inverse of the air entry value (α) and the pore size distribution index (n). For grassland sites, these differences in soil moisture response could also be related to TWI. However, the number of samples analysed was small, and HYDURS-1D did not adequately simulate the redistribution of rainfall. This leads to uncertainties in the results and suggests that further research is necessary. In conclusion, this thesis illustrates how soil hydraulic properties vary spatially due to topography and land cover, and that these differences affect the redistribution of soil moisture, and therefore also the runoff, in the Studibach catchment.

1. Introduction

Soil characteristics influence water storage, infiltration, and runoff responses to rainfall events (Romano and Palladino, 2002). In particular, the spatial redistribution of water during and after rainfall events is highly dependent on soil physical and hydraulic properties, such as soil texture, bulk density, organic matter content, drainable porosity, water retention and hydraulic conductivity, especially in the topsoil (Hartmann et al., 2020; Geroy et al., 2011; Gonzalez-Sosa et al., 2010; Gutmann and Small, 2005). For example, soil texture affects the water retention capacity, infiltration rate, plant available water, and whether rain can infiltrate or becomes surface runoff (Gonzalez-Sosa et al., 2010; Taye et al., 2018). Moisture redistribution is affected by topography due to subsurface lateral redistribution, gravitational effects and variations in solar radiation (Geroy et al., 2011). This in turn affects vegetation cover and soil physical properties, such as the soil organic matter content (Foth, 1990; Stahr et al., 2008; Weil and Brady, 2017). Overland flow can lead to soil erosion and deposition of eroded material in depressions, affecting the soil texture, which also affects the soil hydraulic properties (Weil and Brady, 2017). Therefore, soil (hydraulic) properties will likely vary with topography and knowledge of how they vary with topography is beneficial for understanding hydrological processes, groundwater recharge, contaminant transport, and erosion (Biswas, 2019, Dymond et al., 2017; Gonzalez-Sosa et al., 2010). Furthermore, knowing how water is redistributed in time and space is essential for monitoring the soil water balance and improving soil hydrological models (Biswas, 2019).

This master thesis, therefore, aims to investigate the influence of topography, vegetation, and soil organic matter on soil hydraulic properties. The focus is on the relationship between soil moisture and matric potential, and in particular the drainable porosity and soil water retention. As soil water retention depends on the pore space distribution, soil texture is also investigated. The topographic wetness index (TWI) and slope are used to determine the effect of topography on the soil hydraulic properties. The knowledge of the differences in soil properties are used to predict the differences in water redistribution during rainfall events using the HYDRUS-1D model. This one-dimensional model is designed to simulate the movement of water and solutes through the unsaturated and/or saturated soils based on the Richard's equation (Corona and Ge, 2022; Šimůnek et al., 2013).

Specifically, the research questions of this thesis are:

- 1) How are soil hydraulic properties related to topography?
- 2) Do differences in the soil hydraulic properties affect overland flow, infiltration rates, and soil moisture redistribution during heavy rainfall events?

This thesis tests the following hypotheses:

- 1) Soil organic matter content, drainable porosity and water retention curves vary with topography due to the relation between soil type, vegetation cover and topography.
 - a) Soil organic matter content increases with increasing TWI values.
 - b) Drainable porosity decreases with increasing TWI values.
 - c) Water retention capacity increases with increasing TWI values.
- 2) The observed differences in soil hydraulic properties lead to considerable differences in the amount of infiltration and overland flow, as well as the distribution of soil moisture throughout the soil profile.

This thesis introduction is followed by a background section explaining important concepts, defining specific terms, and an introduction of the study site. Afterwards, the methods used are described, including the field measurements, laboratory analysis, data analysis and model application. The laboratory and simulation results are described and then discussed and interpreted. Finally, the conclusion is followed by a reference list and an appendix with additional graphs and tables.

2. Background

2.1. Catena concept

The catena concept describes the sequence of soil and profile properties along a hillslope that are influenced by topography and drainage (Foth, 1990; Stahr et al., 2008; Weil and Brady, 2017). Figure 1 illustrates a soil catena with poorly developed soils in steep areas compared to the flatter uphill and downhill areas (Foth, 1990; Weil and Brady, 2017). On steep slopes, soil material is more easily eroded, fine soil particles such as silt and clay and organic-rich material are transported from uphill to downhill areas (Foth, 1990; Stahr et al., 2008; Weil and Brady, 2017). Therefore, soil texture and soil organic matter (SOM) often differ along the profile, with more fine soil particles and higher organic matter content in downslope areas (Foth, 1990; Pachepsky et al., 2001; Weil and Brady, 2017). Furthermore, topography can influence soil-water interactions. Soils on steep slopes are generally well-drained, while water accumulates in downhill areas, resulting in poorly drained depressions (Weil and Brady, 2017). Hence, higher water availability and organic matter content in the downhill area increases vegetation cover (Janzen et al., 2002; Pei et al., 2010; Starr et al., 2000; Weil and Brady, 2017), except if the downhill area is so wet that wetlands form in these areas. Wet conditions increase vegetation cover, helping to increase the thickness of the A horizon in soils (Weil and Brady 2017). On steep slopes, soil thickness is lower (Foth, 1990; Weil and Brady, 2017).

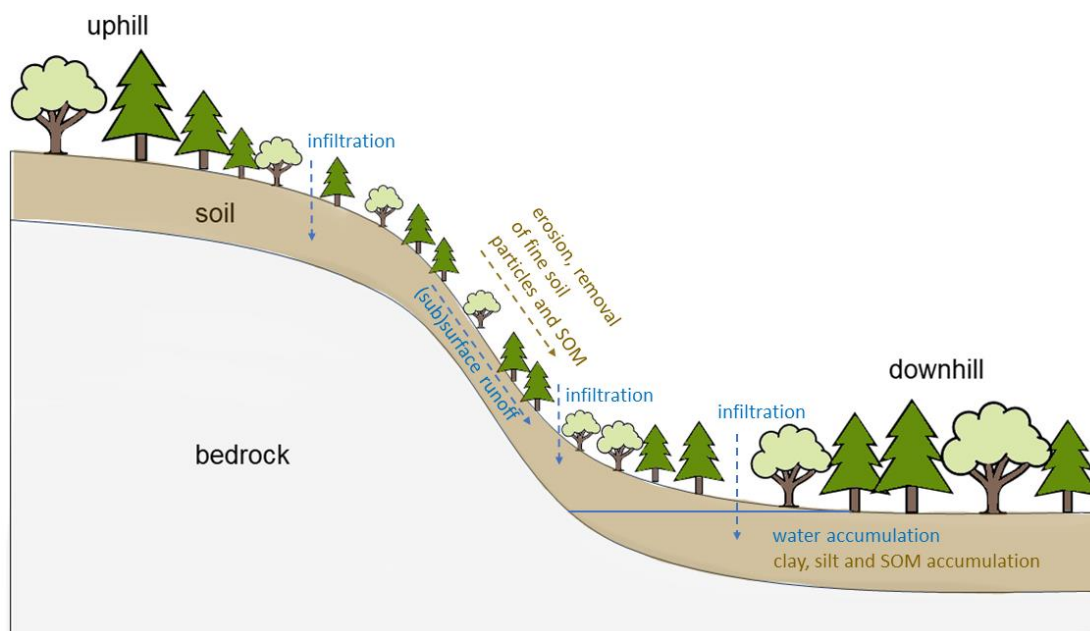


Figure 1: Illustration of soil catena according to descriptions of Dougherty et al. (2004), Foth (1990), Pachepsky et al. (2001), Stahr et al. (2008), and Weil and Brady (2017). Own figure.

The topographic wetness index (TWI) describes the effects of topography on soil moisture within a soil catena (Beven and Kirkby, 1979; Winzeler et al., 2022). It can be calculated using the following formula:

$$TWI = \ln\left(\frac{a}{\tan(b)}\right)$$

and depends on the upslope contributing area per unit contour length (α) and the local slope (b) (Beven and Kirkby, 1979). The local slope is assumed to be a proxy for the local hydraulic gradient and thus describes the drainage (Beven and Kirkby, 1979; Rinderer et al., 2014; Winzeler et al., 2022). A low TWI value indicates a well-drained area due to steep topography and a small contributing area. In contrast, a high TWI indicates a poorly drained area with flat slopes and a significant contributing area. Several studies have linked TWI to different hydrological characteristics, such as soil moisture, groundwater response, and soil organic matter (Pei et al., 2010; Riihimäki et al., 2021; Rinderer et al., 2014; Winzeler et al., 2022). However, good performance of the indicator depends on several physical factors, such as near-surface groundwater levels, wet conditions or non-flat terrain (Pei et al., 2010; Rinderer et al., 2014).

2.2. Soil physical properties

2.2.1. Soil texture

Soil texture is a physical soil property that describes the grain size distribution of the soil particles and, thus, the proportion of sand, silt, and clay (Foth, 1990; Hillel, 2003; Selker and Or, 2019; Weil and Brady, 2017). The grain size distribution defines the coarseness or fineness

Table 1: Grain size fractions with ranges of grain sizes (USDA, 2017).

Grain size fraction	Range of grain sizes (µm)		
Very coarse sand	2000	–	1000
Coarse sand	1000	–	500
Medium sand	500	–	250
Fine sand	250	–	100
Very fine sand	100	–	50
Coarse silt	50	–	20
Fine silt	20	–	2
Clay	2	–	< 2

of soil (Foth, 1990). The largest soil particle after removing rocks and gravel (>2 mm) is a sand particle (50 – 2000 µm), divided into very coarse, coarse, medium, fine, and very fine sand (Table 1). The next smaller particle size is silt (2 – 50 µm), which can be divided into coarse and fine silt. Clay particles are smaller than 2 µm (USDA, 2017). Clay particles have a large surface area, allowing them to adsorb more water than sand or silt (Foth, 1990; Hillel, 2003). Soils with different sand, silt and clay proportions can be classified into 12 different texture classes (USDA, 2017; Figure 2). Loam is commonly used to describe soil texture classes that contain a mixture of sand, silt, and clay particles (Weil and Brady, 2017).

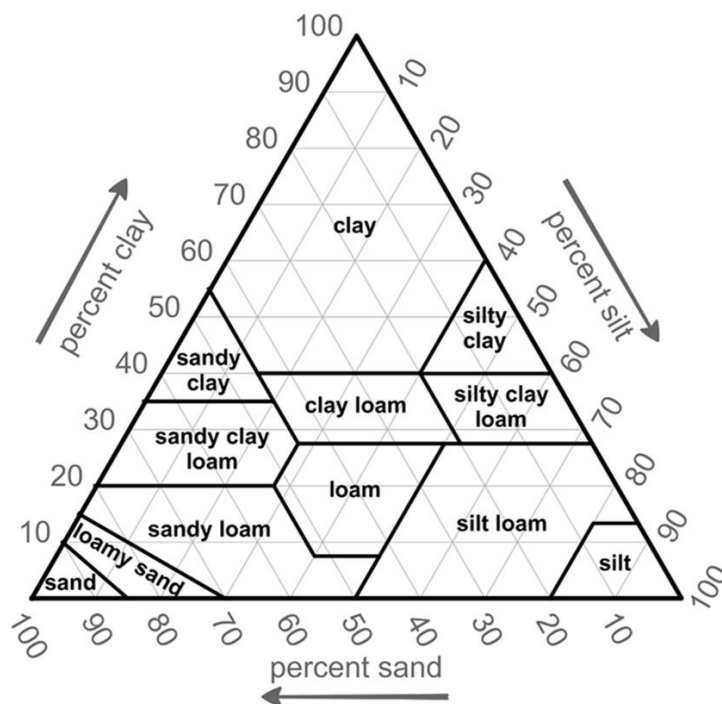


Figure 2: Soil texture triangle according to USDA classification.

Soil texture is related to topographic variables, such as slope and elevation (Rawls and Pachepsky, 2002; Taye et al., 2018). As explained in the catena concept, the differences in soil texture are mainly due to erosional processes, as slopes promote the removal and transport of fine material. This results in soils with coarser soil textures on steep slopes and soils with finer textures in the flatter downslope areas (Pachepsky et al., 2001; Taye et al., 2018).

Soil texture affects water infiltration through micropores (Selker and Or, 2019; Alaoui et al., 2011; Basset et al., 2023; Hartmann et al., 2020; Lohse and Dietrich, 2005; Taye et al., 2018). Infiltration rates are higher for soils with a coarse soil texture (e.g. sandy soils) due to the larger pores between soil particles; they also drain faster than fine-textured soils (Hartmann et al., 2020; Lohse and Dietrich, 2005; Taye et al., 2018). However, soil structure can modify the effect of soil texture on infiltration. Infiltration can be higher in fine textured soils than in coarse

textured soils due to a more stable and developed soil structure (Basset et al., 2023). Fine soil particles promote aggregation due to high binding forces caused by the large surface area per volume, which improves soil structure (Basset et al., 2023). Furthermore, the influence of macropores (pores made by roots, earthworms, cracking and so on) may also change the effect of texture on infiltration, as macropores promote vertical preferential flow and thus infiltration (Selker and Or, 2019). Jarvis (2013) found in a large study that the soil hydraulic conductivity is only weakly related to texture but rather to land use, soil organic matter and bulk density.

2.2.2. Soil organic matter

Soil organic matter (SOM) includes all organic components in the soil, such as plant residues, soil biomass and other organic compounds (Weil and Brady, 2017). It is produced by primary producers (e.g. plants) and consumed by soil organisms (Foth, 1990; Weil and Brady, 2017). SOM content generally decreases with soil depth (Weil and Brady, 2017). As SOM is mainly composed of soil organic carbon (SOC), SOC is often used as a quantitative measure for SOM (Merilä et al., 2010; Weil and Brady, 2017). SOM contributes to soil structure by binding soil particles (Weil and Brady, 2017). It also affects soil water retention by increasing the soil water holding capacity and plant available water (Evrendilek et al., 2004; Foth, 1990; Weil and Brady, 2017). Furthermore, it provides nutrients to plants (Evrendilek et al., 2004; Weil and Brady, 2017).

Previous research has found a correlation between vegetation cover and SOM, and a higher SOM and soil organic carbon content in soils with natural forests than grasslands (Jarvis et al., 2013; Morais et al., 2019; Pirastru et al., 2013). However, other studies found no statistical difference in SOM content between forest and grassland (Celik, 2005; Evrendilek et al., 2004). Previous research agrees that soils under cultivated or grazed land have lower organic matter contents than forest and grassland soils (Evrendilek et al., 2004; Gonzalez-Sosa et al., 2010) due to compaction, reduction of the organic-rich top layer (Celik, 2005; Alaoui et al., 2011; Pirastru et al., 2013), destruction of soil aggregates and accelerated decomposition of SOM (Evrendilek et al., 2004). Generally, SOM accumulates in areas with high vegetation cover due to increased litter input (Starr et al., 2000; Pei et al., 2010).

The relationship between topography and SOM has also been investigated in previous studies. Slope and SOM/SOC were found to be correlated (Fissore et al., 2017; Fu et al., 2004; Moore et al., 1993). Schwanghart and Jarmer (2011), Moore et al. (1993), and Pei et al. (2010) found

a positive correlation between SOC and TWI (Figure 3). Erosion processes, such as wind and water erosion, affect the distribution of SOM by eroding material on steep terrain and depositing it downslope on flat terrain (Berhe et al., 2008; Fissore et al., 2017; Wang et al., 2009; Pei et al., 2010). Where material accumulates, SOC may be buried and thus protected from decomposition, whereas at erosional sites, SOC may be exposed to decomposition (Berhe et al., 2012; Fierer et al., 2003; Fissore et al., 2017). In addition, higher clay contents in accumulation areas could increase soil stability and thus reduce SOM decomposition (Basset et al., 2023; Green et al., 2000). Furthermore, very high moisture content in poorly drained depressions often reduces microbial activity by reducing oxygen levels, which leads to a slower decomposition and thus, higher SOM contents (Sierra et al., 2017).

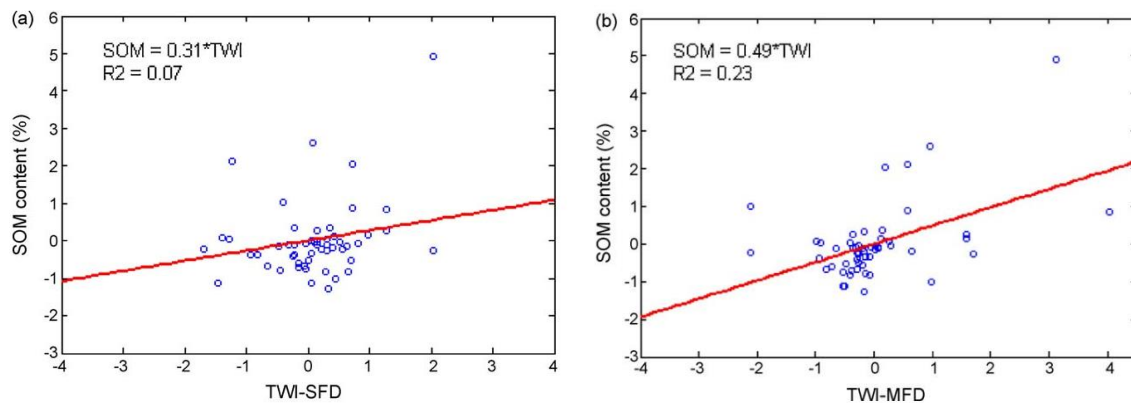


Figure 3: Positive correlation between SOM and TWI, calculated using the single-flow-direction (SFD) and multiple-flow-direction algorithm (MFD) for Mollisol soils in China (A-horizon). Both linear regressions are statistically significant (Pei et al. 2010).

Infiltration is influenced by SOM, as SOM increases aggregate stability and pore formation (Basset et al., 2023; Nyamadzawo et al., 2007; Jemai et al., 2012; Hartmann et al., 2020; Schwanghart and Jarmer, 2011). Infiltration rates increase with soil organic carbon, as shown by previous research (Franzluebbers, 2002; Basset et al., 2023).

2.3. Soil hydraulic properties

Soil hydraulic properties include water retention, drainable porosity, and hydraulic conductivity (Hartmann et al., 2020, Hillel, 2003). Water retention describes the storage capacity of the soil and affects the amount of water available to plants (Ashok et al., 2020; Bormann and Klaassen, 2008; Hartmann et al., 2020; Jarvis et al., 2013; Lin, 2010). The drainable porosity and hydraulic conductivity affect the response to rainfall events and thus infiltration and runoff (Gonzalez-Sosa et al., 2010). Land use and vegetation cover strongly influence these properties (Bormann and Klaassen, 2008).

2.3.1. Soil water retention curves (SWRC)

Soil water retention curves (SWRC) or pF curves describe the relationship between the soil matric potential and volumetric soil moisture content (Figure 4) (Geroy et al., 2011). It shows the amount of water that is stored in the soil at different matric potentials and the change in matric potential when soil water is removed (or vice versa) (Hartmann et al., 2020). Matric potential, sometimes referred to pressure head, is often plotted on a logarithmic scale, defined as pF (e.g. -10^2 hPa = pF of 2) (Kirkham, 2005; UMS, 2015). Figure 4 shows that moisture content decreases non-linearly with increasing pF values. Before air starts to enter the largest soil pores, the air-entry pressure must be exceeded (Selker and Or, 2019). This critical pressure is visible in Figure 4 as a horizontal line and differs according to the pore size (Selker and Or, 2019). At a pF of 4.2, the water is held so tightly by matric forces that the water is no longer available to plants (METER, 2021; Selker and Or, 2019). This is called the *wilting point* (Figure 4) (Selker and Or, 2019). *Field capacity* is the moisture content after gravity drainage has stopped (i.e., when the soil has reached a certain tension, and all macropores have been emptied by gravitational forces; Selker and Or 2019; Weil and Brady 2017). For soils with a high groundwater level, this is the case at a pF of 1.8, and for soils with a low groundwater level, it is at a pF of 2.5 (METER, 2021). At this point, matric forces hold the remaining water in the soil pores (Weil and Brady, 2017). The soil water content between the field capacity and the wilting point is referred to as *plant-available soil water* (Selker and Or, 2019).

The shape of the water retention curve strongly depends on the pore size distribution (Selker and Or, 2019; Weil and Brady, 2017). Selker and Or (2019) explained this relationship conceptually by first converting particle size (Figure 5a) to pore size (Figure 5b), and mass fraction (Figure 5a) to volume fraction (Figure 5b). The ratio remains the same. After equating pore size (Figure 5b) to pore pressure via the equation $h = -2\sigma/r$, where h is the matric potential, σ the surface tension, and r the radius (Figure 5c) and volume percent V (Figure 5c) to moisture content (Θ) by multiplying by the porosity (Figure 5d), a soil water retention curve is constructed from a particle size distribution curve (Selker and Or, 2019).

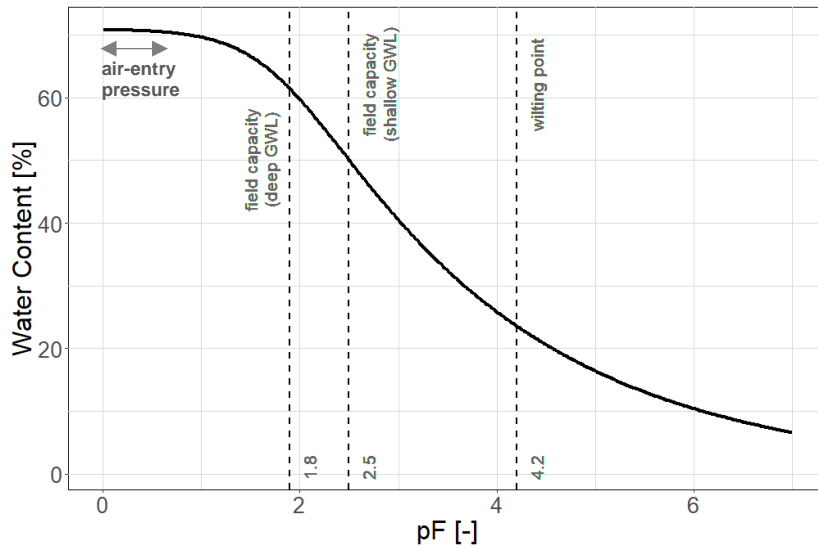


Figure 4: Soil water retention curve showing the relation between the volumetric soil moisture content (water content) on the y-axis and soil matric potential (pF) on the x-axis, with the moisture content at field capacity for sites with a shallow ground water level (shallow GWL) marked at a pF of 1.8 and for sites with deep ground water level (deep GWL) at a pF of 2.5, and the wilting point at a pF of 4.2.

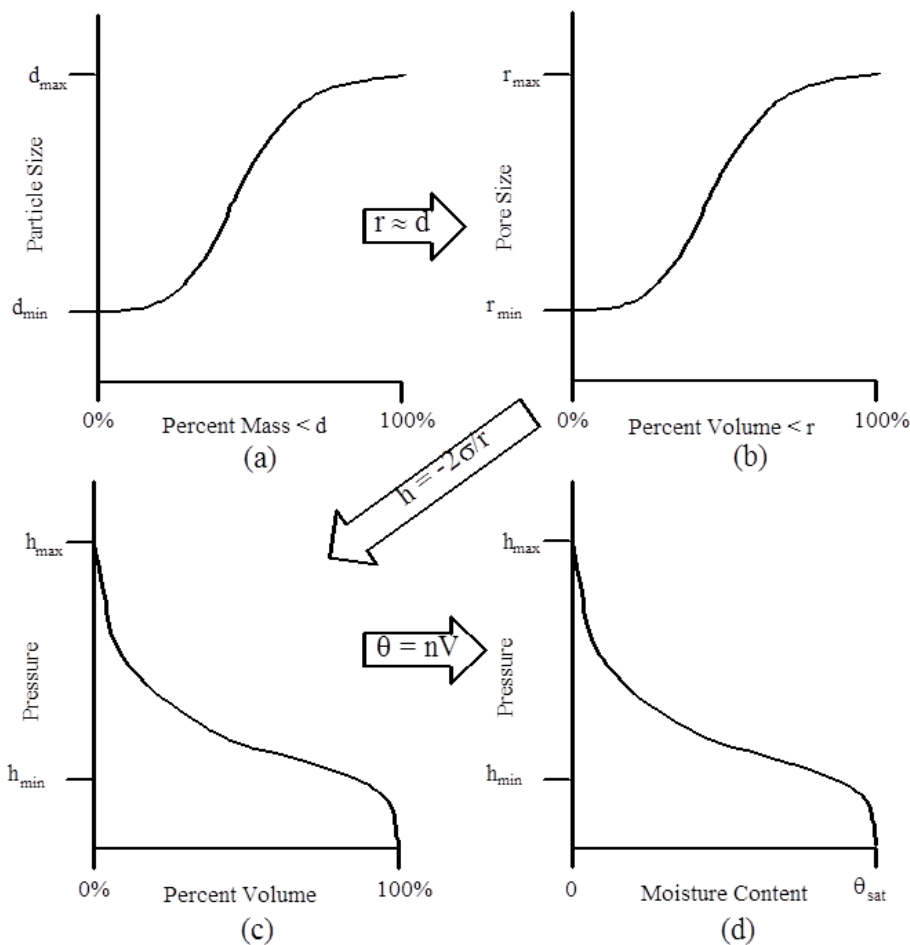


Figure 5: Relation of soil water retention curve to pore size distribution (Source: Selker and Or, 2019).

As the water retention curve (SWRC) depends on the particle size distribution, the shape of the SWRC is influenced by soil texture (Selker and Or, 2019; Weil and Brady, 2017). Small soil pores, such as those found in clay, can retain approximately 50% of soil water through capillarity and adhesive forces (Weil and Brady, 2017). Therefore, soils with a high proportion of clay, such as clay soils, have high moisture content at saturation, and the volumetric moisture content gradually decreases with a higher (more negative) matric potential (Figure 6) (Hillel, 2013; Selker and Or, 2019). Sandy soils have larger pores and adhesive forces are lower, which means that for a given matric potential, there is less water in the pores than in clay or silt soils (Hillel, 2013; Weil and Brady, 2017). When all the macropores are emptied, there is not much water left in the soil. For these reasons, SWRC for sand do not reach as high volumetric moisture content as clay soils, and the moisture content decreases rapidly at low matric potentials until it reaches low levels (Figure 6) (Hillel, 2013; Weil and Brady, 2017).

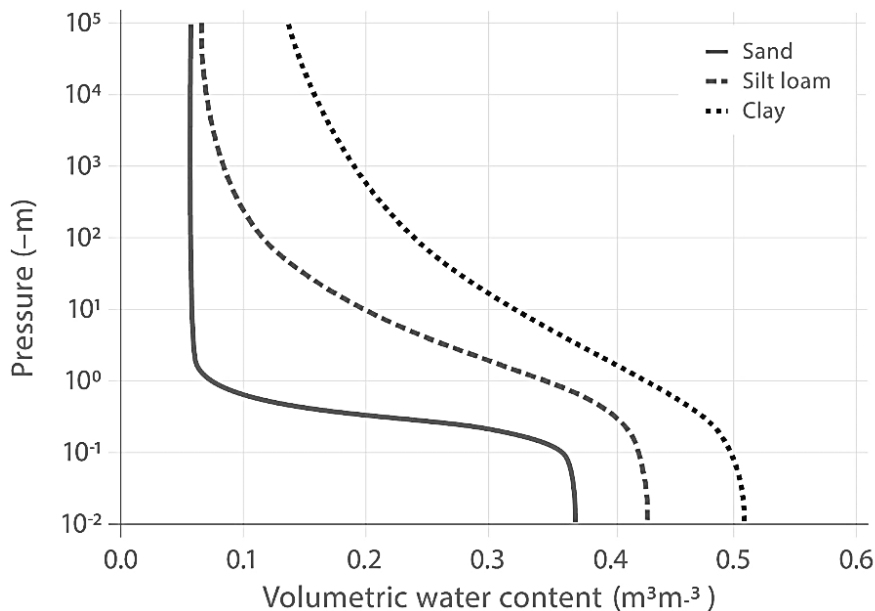


Figure 6: Typical soil water retention curves with different soil texture classes (Source: Selker and Or, 2019).

Vegetation cover often does not affect soil texture, but it affects other soil physical properties, such as porosity, bulk density and organic matter content (Dlapa et al., 2020; Pirastru et al., 2013). SWRCs vary with these properties, because soil physical properties affect water retention, especially near saturation (Agnese et al., 2011; Pirastru et al., 2013). Thus, several studies have shown that water retention differs with vegetation cover (Dlapa et al., 2020; Pirastru et al., 2013; Saha et al., 2015). According to Pirastru et al. (2013), soils with natural vegetation (e.g. forest, natural grassland) have a higher organic matter content, higher porosity, more stable macropores, and lower bulk density than soils affected by human activities (e.g. cultivated or grazed grassland). They also found that forest soils have a higher water retention

at low (near-zero) tensions than grassland soils due to higher organic matter content (Figure 7), while Saha et al. (2015) found a higher moisture content in grassland soils. Fine roots in grassland soils can increase soil porosity and water-holding capacity (Schenk and Jackson, 2002). However, forests are also characterised by high porosity and low bulk density due to high organic inputs, litter cover, and also high densities of plant roots and soil fauna, which are responsible for stable macropores (Alaoui et al., 2011; Lee and Foster, 1991; Pirastru et al., 2013; Wang et al., 2013). Macropores are important for preferential flow and infiltration in highly saturated topsoils (Dlapa et al., 2020; Pirastru et al., 2013; Selker and Or, 2019).

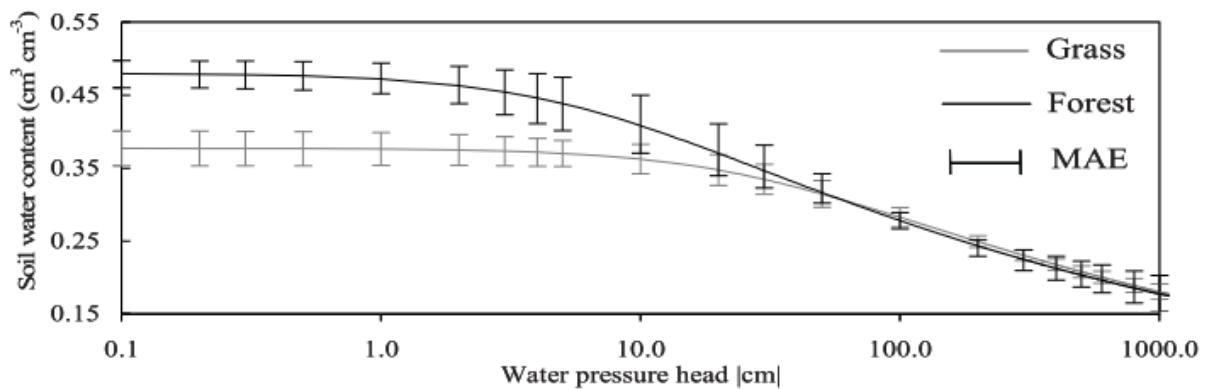


Figure 7: Soil water retention curves and mean absolute errors (MAE) in grassed and forest soils (Source: Pirastru et al., 2013).

2.3.2. Drainable porosity

Drainable porosity (DP) is the volume of water that can be drained by gravity from a saturated soil, i.e., it is the difference between porosity and the soil moisture at field capacity (Gregory et al., 1999; Ottoni et al., 2022). It is defined by the volume of water drained from a soil per unit surface area in response to changes in the water table (Hilberts et al., 2005; Pali et al., 2014; Skaggs et al., 1978; Taylor, 1960).

Figure 8 illustrates the relationship between drainable porosity and soil water retention. Differences in water retention are particularly large near saturation (Weiler and McDonnell, 2004). Soils with a steep SWRC between moisture content at saturation and field capacity (in Figure 8 at 100 cm) have a high drainable porosity. Water retention between 0 and 100 kPa is affected by soil structure (Weil and Brady, 2017). Thus, the difference between the water retention curves of soils with high and low drainable porosity is due to differences in the soil structure, with high drainable porosity soils having more macropores (Weiler and McDonnell, 2004). Furthermore, an intact aggregate structure, for example, through a high SOC content, will increase the moisture content at saturation and lower the initial decrease in moisture content

at a low matric potential (Dlapa et al., 2020; Weil and Brady, 2017). In other words, it will also lead to a higher drainable porosity.

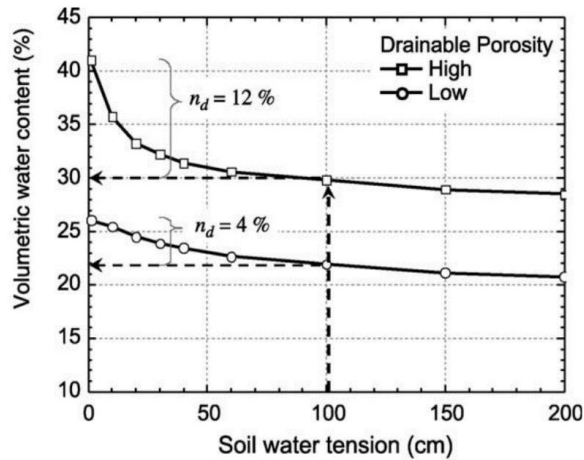


Figure 8: Relation of drainable porosity (low and high) to soil water retention curves (source: Weiler and McDonnell, 2004).

Weiler and McDonnell (2004) investigated how drainable porosity affects the hydrological responses and found that the increase in the groundwater is smaller for soils with a high drainable porosity. This results not only in greater channelling of subsurface lateral flow but also in more event water. They explain the higher proportion of event water by the fact that soils with a high drainable porosity have less water stored in the soil prior to the event. They also found that the depth of saturation was lower for soils with a high drainable porosity and that soils with low drainable porosity had higher moisture contents in the unsaturated layer and higher water table fluctuations than soils with a high drainable porosity. According to their study, the higher water table variations lead to more variations in runoff concentrations.

2.4. Hydrological models

A hydrological model is a simplification of nature to predict and better understand hydrological processes such as infiltration, subsurface lateral flow, surface runoff, and so on (Beven, 2012; Devi et al., 2015; Islam, 2011). Physically based hydrological models provide a mathematical representation of water movement based on partial differential equations, such as the Richards equation (Abbott et al., 1986; Islam, 2011; Song et al., 2020; Ventrella et al., 2019). The Richards equation is based on Darcy's law and the concept of mass conservation. It can be solved using soil hydraulic parameters, such as soil matric potential, hydraulic conductivity and soil moisture content (Abbott et al., 1986; Beven, 2012; Brunone et al., 2003; Devi et al., 2015; Van Dam and Feddes, 2000).

According to Maskey (2022), the formula of the Richards equation with soil moisture content as the dependent variable is as follows:

$$\frac{\partial \theta}{\partial t} = \frac{\partial}{\partial z} \left(K(\theta) \frac{\partial \psi}{\partial z} \right) + \frac{\partial K(\theta)}{\partial z} - W_s$$

where θ is the soil moisture content, ψ is the local matric potential, $K(\theta)$ is the hydraulic conductivity as a function of soil moisture, and W_s is the water uptake by plants (Maskey, 2022). HYDRUS-1D is a physically based program that numerically solves the Richards equation for unsaturated and saturated soils in a one-dimensional vertical soil column (Corona and Ge, 2022; Šimůnek et al., 2013). This model is based on soil hydraulic parameters such as saturated conductivity (K_s), saturated moisture content (θ_s), residual moisture content (θ_r), inverse of air entry value (α , l/m), and pore size distribution index (n) (Šimůnek et al., 2013; Song et al., 2020). The last four parameters describe the SWRC based on the van Genuchten's soil water retention equation (Van Genuchten, 1980), which is based on Mualem's pore size distribution model (Mualem, 1976):

$$\theta(\psi) = \begin{cases} \theta_r + \frac{\theta_s - \theta_r}{[1 + |\alpha\psi|^n]^m} & \psi < 0 \\ \theta_s & \psi \geq 0 \end{cases}$$

$$K(\psi) = K_s S_e^l [1 - (1 - S_e^{1/m})^m]^2$$

$$m = 1 - 1/n, \quad n > 1$$

Where S_e is the effective saturation and m is the pore size distribution term (Stewart et al., 2013). For many soils, 0.5 is a reasonable estimate of the pore connectivity parameter (l) (Mualem, 1976; Šimůnek et al., 2013).

According to Baumhardt et al. (1990), saturated hydraulic conductivity, pore size distribution parameters and water entry value have the most pronounced influence on the model results. Other parameters, such as the residual moisture content, have little influence on the model results (Song et al., 2020). The saturated conductivity K_s is a key parameter because it is highly variable and strongly influences infiltration (Šimůnek et al., 2013; Ventrella, 2019). High

conductivity values favour water infiltration (Dussaillant et al., 2004). The simulated infiltration is lower with decreasing K_s (Baumhardt et al., 1990 and 2004). Infiltration into the permeable layer can raise the water table, promoting subsurface lateral flow (Weiler and McDonnell, 2004). Hopp and McDonnell (2009) found that for subsurface lateral flow to occur, the difference in K_s between the permeable and inhibitory soil layers must be small.

3. Study site

3.1. Alptal

The Alptal is a mountainous catchment located in the Canton of Schwyz, Switzerland, in the pre-Alps, which lies between the Central Swiss Plateau and the Swiss Alps (Ragettli et al., 2021; Stähli et al., 2021; Van Meerveld et al., 2018). It is a research site for many institutes and is particularly interesting to hydrologists because the high precipitation and low permeability soils lead to rapid streamflow responses (Stähli et al., 2021). There have been many hydrological studies at this site (Stähli and Badoux, 2018; Stähli et al., 2021; Van Meerveld et al., 2018). However, so far, a link between soil properties, hydrology and topography has not been established.

The area of the Alptal catchment is 46.4 km². Elevation ranges from 840 to 1898 m a.s.l. (Ragettli et al., 2021). The average slope is 19° (Van Meerveld et al., 2018). The climate is temperate with a mean annual air temperature of 6.7°C at the MeteoSwiss station in Einsiedeln (Ragettli et al., 2021) and a high annual precipitation of 2300 mm/year (Feyen et al., 1996; Van Meerveld et al., 2018; Van Meerveld et al., 2019). The vegetation in the Alptal is heterogeneous, with the steeper slopes mainly covered by forests (silver fir and spruce) and the flatter areas by meadows and wetlands (Ragettli et al., 2021; Van Meerveld et al., 2018; Van Meerveld et al., 2019).

The catchment consists of flysch bedrock (very low permeability sedimentary rock sequence) (Feyen et al., 1996) and is covered by Gleysols (Ragettli et al., 2021; Van Meerveld et al., 2018). Gleysols are soils that are influenced by groundwater and saturated for long periods (FAO, 2015). This leads to reduced (low oxygen) conditions and segregation of Fe and gleyic characteristics (FAO, 2015). As a result, the upper soil is brownish, while the deeper soil is greyish. Gleysols have a low hydraulic conductivity due to high clay and silt content (Figure 9), which prevents deep infiltration (Ragettli et al., 2021; Stähli et al., 2021; Van Meerveld et al., 2018). In the forests, however, the hydraulic conductivity is higher in the upper soil layers due to roots (Van Meerveld et al., 2018). With limited infiltration and high rainfall, groundwater levels are close to the surface (Rinderer et al., 2014; Van Meerveld et al., 2019). Therefore, not only the streams, but also subsurface and surface flows, respond rapidly (e.g. 10 min) and dynamically to high and prolonged precipitation events (Feyen et al., 1996; Fischer et al., 2016; Ragettli et al., 2021; Rinderer et al., 2014; Van Meerveld et al., 2018 and 2019).

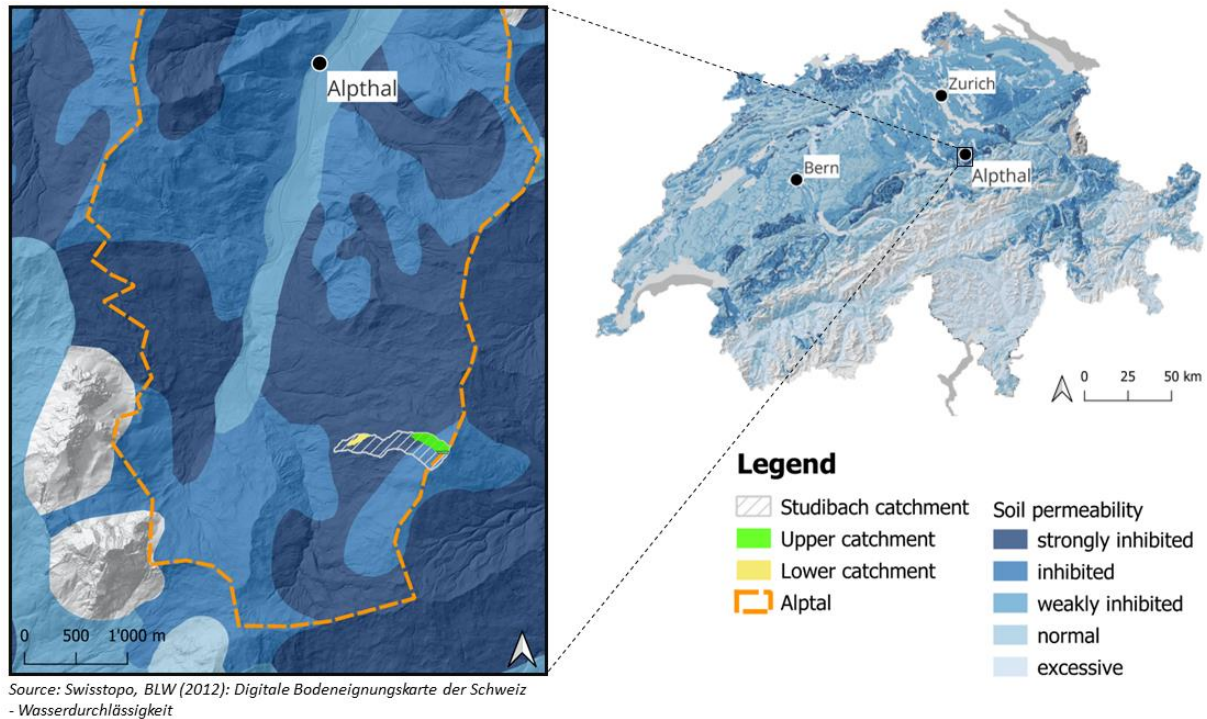


Figure 9: Map of the soil permeability (top 50 cm) in the Alptal based on permeability test in the laboratory and morphologic characteristics of Switzerland (Data: BLW, 2012).

Soil texture in the Alptal varies somewhat with topography. Groundwater levels are near the surface in depressions or under grassland, where the soil has a high carbonate content and consists of about 43% clay, 42% silt, and 15% sand (Rinderer et al., 2014; Schleppi et al., 1998). Groundwater levels are deeper in steeper tree-covered areas with macropores, where the soil consists of 49% clay, 46% silt, and 5% sand (Hagedorn et al., 2001; Rinderer et al., 2014; Schleppi et al., 1998).

Soil moisture is generally high but varies according to topography and vegetation (Van Meerveld et al., 2018). Kollegger (2011) found higher soil moisture in open areas than in forests, and higher soil moisture in depressions than on ridges. According to Rinderer et al. (2014), the topographic wetness index (TWI) is a good indicator of soil wetness in this area. They found that areas with low TWI values ($TWI < 4$) responded only to high-intensity precipitation events, whereas areas with moderate TWI values ($TWI 4-6$) showed a more frequent and stronger groundwater response. Areas with high TWI values ($TWI > 6$) tended to respond quickly but not strongly, as the groundwater level is already near the surface. There, groundwater levels changes lasted for a few days (Rinderer et al., 2014).

3.2. Studibach catchment

The Studibach catchment (0.2 km²) is located in the Alptal at an elevation of 1270 - 1656 m. a.s.l. and has an average slope of 21° (Van Meerveld et al., 2019). Half of the catchment is covered by forest and half by grasslands, wetlands, and meadows (Van Meerveld et al., 2019). There are two sub-catchments, the lower and the upper catchment (Figure 10). The lower catchment is dominated by forest. Wetlands, grasslands, and meadows mainly cover the upper catchment.

The sampling sites used for this thesis were chosen to cover different TWI based on the calculation by Rinderer et al. (2014) for a 5 m Digital Elevation Model (DEM). Seven sites are located in the lower and three in the upper catchment. Slope, TWI, soil layers, and land use vary between the sampling sites (Figure 10; Table 2).

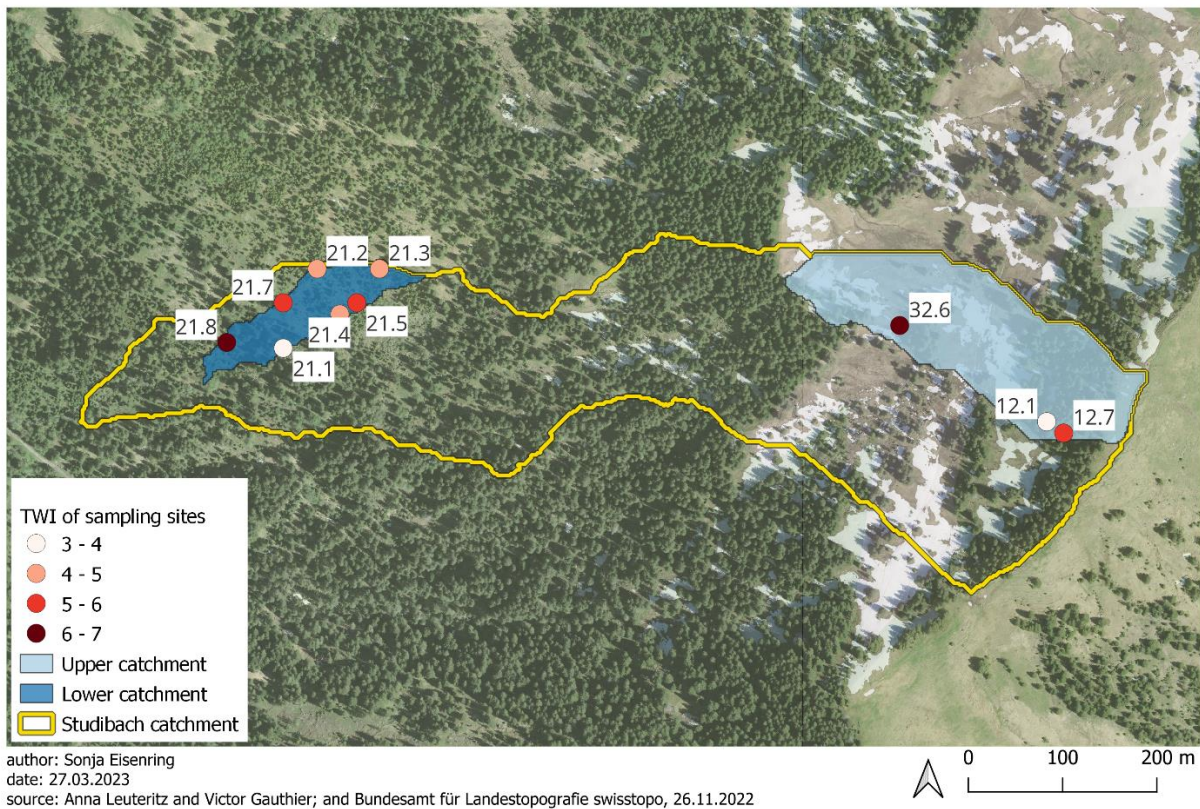


Figure 10: Map of Studibach Catchment with sub-catchments in blue and sampling sites in red shades according to TWI value.

Table 2: Main characteristics of the sampling sites in the Studibach catchment containing the site name, coordinates (WGS1984), elevation, topographic wetness index (TWI) value, slope (data from Rinderer et al., 2014), vegetation, and observed depth of the A and B horizon (data from Anna Leuteritz and Victor Gauthier).

Site	Latitude (°N)	Longitude (°E)	Elevation (m.a.s.l.)	TWI	Slope (%)	Vegetation	A horizon (cm)	B horizon (cm)
21_1	47.03882	8.72088	1327	3.4	15.6	forest	0-10	10-40
21_2	47.03957	8.72137	1354	4.1	21.0	grassland	0-15	15-30
21_3	47.03956	8.72224	1371	4.4	12.6	grassland	0-17	17-32
21_4	47.03913	8.72167	1345	4.8	25.6	forest	0-20	20-40
21_5	47.03924	8.72191	1353	5.2	21.0	forest	0-20	20-40
21_7	47.03920	8.72097	1330	6.0	17.7	forest	0-18	18-35
21_8	47.03888	8.72009	1313	7.0	8.5	grassland	0-15	15-30
12_1	47.03800	8.73152	1609	3.5	33.9	forest	0-10	10-33
12_7	47.03789	8.73175	1614	5.3	29.8	grassland	0-10	10-40
32_6	47.03894	8.72949	1545	6.9	14.8	grassland	0-15	

4. Methods

4.1. Field measurements

Field measurements were carried out between September 06 and 23, 2022. These included soil sampling and soil resistance measurements using a cone penetrometer. Topographic parameters, such as TWI, elevation and slope, had already been measured by Rinderer et al. (2014). Anna Leuteritz and Victor Gauthier have measured overland flow and near-surface flow in the field. They determined the depth of the A and B soil horizon depth at each sampling site when they installed their trenches.

At each site, one soil sample (250ml) was collected from 2-7 cm (e.g., 21_1_1) and one from 10-15 cm (e.g., 21_1_2). A total of 20 soil samples was collected. The samples were stored in a refrigerator until laboratory analysis for grain size determination, measurement of SWRC, and measurement of organic matter using the loss on ignition method.

Soil density and resistance were determined using a cone-penetrometer. Soil resistance was measured every 5 cm to a depth of 1 m at three locations at each sampling site (above, in the middle, and below) using a Handpenetrometer Eijkelkamp (accuracy of $< \pm 8\%$; Eijkelkamp, 2023).

4.2. Laboratory analysis

4.2.1. Soil water retention and drainable porosity

Laboratory analysis included the determination of the soil water retention curves (SWRC) using a Hydraulic Property Analyser (HYPROP 2). Prior to using HYPROP 2, the soil samples were saturated with deionised water. The water in the tension shafts and sensor unit was degassed using the HYPROP refill unit to ensure accurate transmission of the tension (UMS, 2015). Furthermore, the balance and the sensor unit were calibrated. Using the multi-balance mode (one balance per sensor unit), the soil samples were continuously weighed to determine the change in sample mass, while two tensiometers measured the soil water tension in the soil at two depths using an electronic transducer (UMS, 2015; Weil and Brady, 2017). By slowly air-drying the saturated soil samples, LABROS SoilView generated two curves showing the timeseries of the tension (hPa) and sample weight (g). Measurements were stopped when the air entry point of the second tension shaft was reached. It took approximately 12 to 16 days to

generate a complete measurement curve for a sample. Sample 12_7_2 was damaged and could not be measured.

After determination of the SWRC, the soil samples were dried in an oven at 70 °C for two days until the soil was completely dry to determine the dry weight and calculate the bulk density and convert the sample weights to moisture contents.

Drainable porosity was determined from the measured soil water retention curve by subtracting the percentage of moisture content at field capacity for soils with high groundwater levels (pF of 1.8) from the moisture content at saturation.

4.2.2. Soil texture, soil organic matter, bulk density

The dried soil was used to determine the particle size distribution of the soil samples. A hand mortar was used to break up the soil aggregates without destroying the soil particles. Approximately 100 g of dry soil was sieved to <2 mm, and approximately 20-30 g of this fraction was sieved to <250 µm. 5 g of the <250 µm fraction was then mixed with 20 ml of distilled water and 20 ml of 0.5% sodium hexametaphosphate (NaPO₃)₆ solution. Using a Bandelin Sonoplus HD 2070 ultrasonic instrument. The remaining aggregates in the soil liquid were comminuted for 5 minutes at an amplitude of 70% with 5 cycles. Grain sizes smaller than <250 µm were then measured using low-energy X-rays with a SediGraph III Plus. Combining the dry sieve and SediGraph grain size distributions resulted in a grain size distribution curve (Figure A2). The USDA grain size boundaries were used to determine soil texture (Table 1; Figure 2). Due to very high organic matter contents, the soil texture of some samples (21_8_1, 12_1_1 and 12_7_2) could not be measured for technical reasons.

The Loss on Ignition (LOI) method was used to determine the organic matter content. For each sample, 2 g of dry soil (< 2mm) was exposed to a high temperature (550°C). Thus, the organic matter content of the soil was combusted. The difference in weight before and after combustion was then used to calculate the organic matter content.

Soil bulk density (ρ) was calculated from the ratio of the mass of the dry soil (M) to the volume of the sample cylinder (V) (Selker and Or, 2019). The volume of the sample cylinder was 250 cm³.

$$\rho = \frac{M}{V}$$

4.3. Data analysis

4.3.1. Soil water retention curve

The LABROS SoilView analysis tool produced a soil water retention curve showing the volumetric moisture content and soil tension. The moisture content was calculated using the dry soil weight. An additional data point could be generated with the air entry point. The original van Genuchten-Mualem model was used to fit the curves.

4.3.2. Statistical analysis

Data were analysed in R to identify correlations between soil physical and hydraulic properties, organic matter content, and topography. Due to the small sample size (< 30), non-parametric statistical tests were used. Spearman's rank correlation (r_s) was used to investigate the correlation between two variables, for example, soil organic matter content and TWI (Table A2). The Mann-Whitney U test was used to test whether the means values for two groups were significantly different, e.g. soil organic matter content in 2-7 cm and 10-15 cm soils.

4.4. Model analysis

The HYDRUS-1D model was used to simulate the partitioning of rainfall into overland flow and infiltration, and the redistribution of soil moisture throughout the soil profile for two different rainfall events; one large rainfall event from 19.08.2022 and one high-intensity event from 24.06.2022 (Table A3 and A4). These two events were 101 and 37 mm in size, had an average intensity of 4.6 and 4.2 mm/h, and a maximum intensity of 4.2 and 10.5 mm/10min respectively. The high-intensity event is more likely to exceed the soil infiltration capacity and lead to infiltration excess or Horton overland flow. In contrast, the large rainfall event with a longer duration is more likely to result in saturated overland flow.

In the model, a 50 cm deep soil with three different soil layers was created for each site (Figure A1c and Table A1). The van Genuchten-Mualem model was used as the soil hydraulic model (Figure 11). The model uses soil hydraulic parameters, including residual and saturated soil moisture content, alpha, n, and hydraulic conductivity (K_s) (Section 2.4; Table A1). The deepest soil layer was assumed to be clay, for which HYDRUS-1D provided the parameter values, as no measurements were taken at this depth. The parameters of the upper two soil layers, were determined by the van Genuchten-Mualem model in LABROS SoilView. The residual water

parameter was assumed to be the moisture content at the wilting point (pF 4.2). For saturated hydraulic conductivity, the average K_s value for forest was used for the first soil layer of forested sites, and the average value for grassland was used for the first soil layer of grassland sites. These data were collected in the field by Maartje Wadman, MSc student. Although K_s changes exponentially with depth, the average K_s values from layers one and three were used for the second soil layer, as this layer still has roots, but not as many as in the top layer. The tortuosity parameter (l) was set to 0.5 (-) for all soil layers and sites (Table A1).

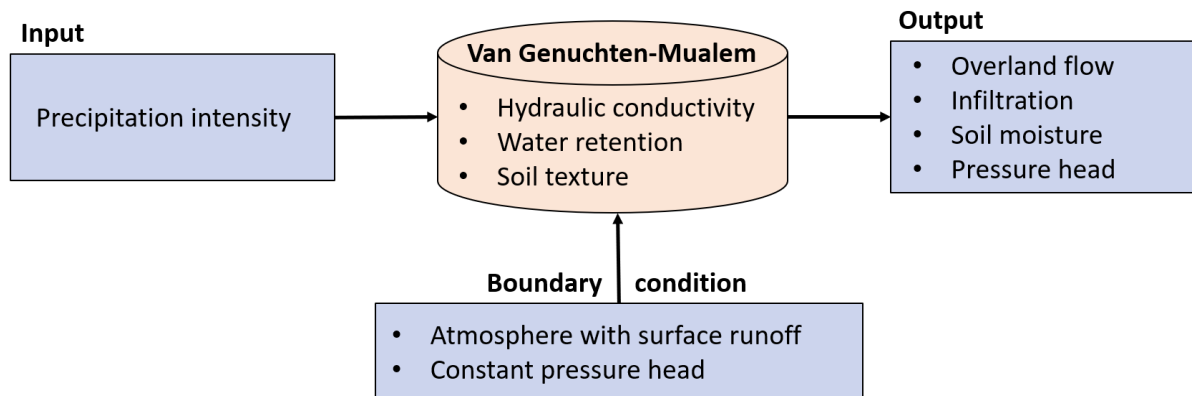


Figure 11: Illustration of HYDRUS-1D model components.

An atmospheric boundary condition with surface runoff was chosen as the upper boundary condition. A constant pressure head was used as the lower boundary condition to facilitate comparison of the effect of the soil hydraulic properties on infiltration and overland flow rates. The initial pressure head ranged from 0 cm at the bottom of the soil to -50 cm at the top of the soil (Figure A1a). The model was run for 250 hours, starting with a small rainfall event to fill the soil water storage, followed by a long period without rainfall. At 100 hours, the events started. For this, the rainfall intensity measured at Erlenhöhe was used for 19.08.2022 and 24.06.2022 (Table A3 and A4). An evaporation rate of 0.004 cm/h was assumed for the entire period. Soil moisture and matric potential was simulated and plotted at 10 different soil depths (Table A1b).

5. Results

5.1. Soil properties

5.1.1. Soil bulk density and soil resistance

Soil bulk density differed between the sampling sites and depths, ranging from 0.15 to 0.86 g/cm³ (Table 3). Generally, soil bulk density was higher at 10-15 cm depth than at 2-7cm depth; this difference was not statistically significant (p=0.2526). Sites 21_7 and 32_6 had lower soil bulk density at deeper depth.

Table 3: Soil bulk density in g/cm³ for each sampling site at both depths.

Site	Soil bulk density (g/cm ³)	
	2 – 7 cm	10 – 15 cm
21_1	0.45	0.66
21_2	0.43	0.46
21_3	0.49	0.63
21_4	0.57	0.86
21_5	0.57	0.64
21_7	0.46	0.16
21_8	0.21	0.23
12_1	0.15	0.55
12_7	0.26	-
32_6	0.53	0.38

At most sites, the mean soil resistance was high near the surface and decreased at about 5 cm (Figure 12). After 5 cm, it mainly increased with depth, except at 12_1 and 32_6, where the resistance remained similar with depth, and 21_5, where the mean resistance was low at depth. At sites 21_1 and 21_3, the observed end of the soil horizons matched the measured mean resistance, with low resistance at the end of the A horizon and increasing resistance at the end of the B horizon. However, this could not be observed for the other sampling sites.

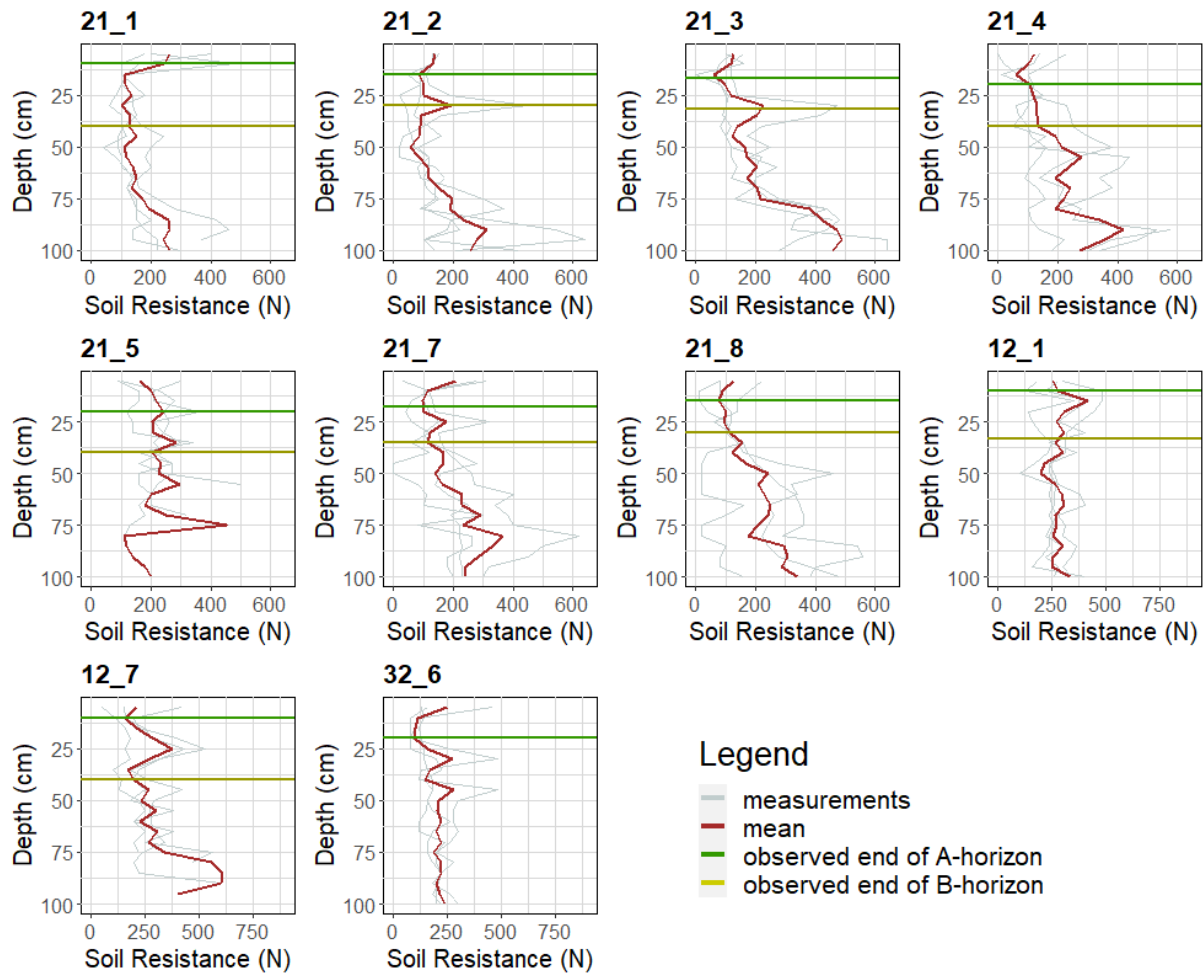


Figure 12: Mean soil resistance as a function of depth below the surface (red), the three individual measurements (gray), and the observed depth of the bottom of the A and B horizons (green).

5.1.2. Soil texture

All samples had a similar soil texture and a closely related texture class: clay, silty clay, clay loam and silty clay loam. The clay content varied between 30 - 60 %, the silt content between 30 - 50 %, and sand content between 5 - 25 %. There were two exceptions: samples 12_1_2 and 21_8_2 (Figure 13). These two samples had a much lower clay fraction and were characterised as silty loam (clay: 10-20%; silt: 50-70%, and sand: 20-30%). There was no clear trend in grain size distribution with TWI at 2-7 cm and 10-15 cm below the soil surface (Figure A2). However, the Spearman rank correlation between clay fraction and TWI was statistically significant when both depths were combined ($p=0.0188$).

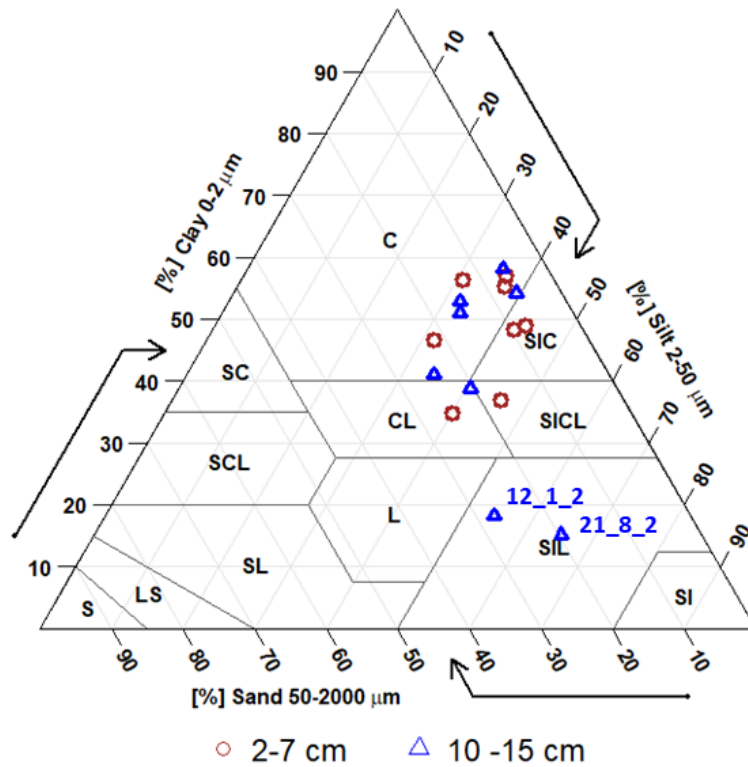


Figure 13: Soil texture of the measured samples in a soil texture triangle (S = sand, LS = loamy sand, SL = sandy loam, SCL = sandy clay loam, SC = sandy clay, L = loam, CL = clay loam, SIL = silt loam, SI = silt, SICL = silty clay loam, SIC = silty clay, C = clay). 12_1_2 and 21_8_2 are marked because their positions differ from the others.

5.1.3. Organic matter

The SOM values were similar, but slightly higher at 2-7 cm than at 10-15 cm (Figure 14). However, this difference was not statistically significant (Table A2). At 2-7 cm, two samples are considered outliers (12_1_1 and 21_8_1) and had the highest SOM values of around 60%. There was also no statistically significant correlation between SOM and TWI or slope for either soil depth (Table A2). However, except for sample 12_1_1 (2-7 cm), there was a trend of increasing SOM content with increasing TWI and decreasing SOM content with increasing slope (Figure 14). This trend was more pronounced in 10-15 cm depth, possibly because the variance of SOM was higher at 10-15 cm than at 2-7 cm. Although also not statistically significant different (Table A2), there was also a trend of higher SOM content and SOM variability in grassland soils than forest soils (Figure 15).

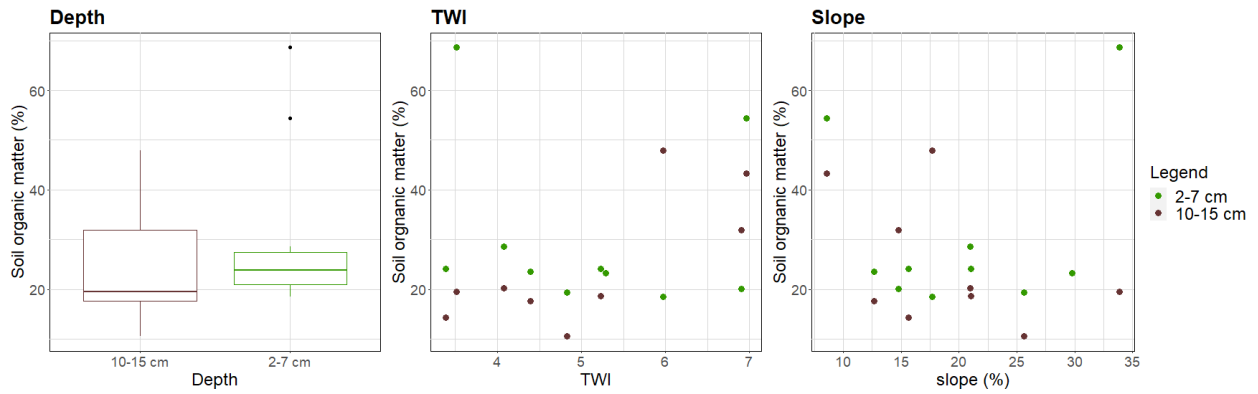


Figure 14: Box plots of soil organic matter at both soil depths (left), and the relations between soil organic matter and TWI (middle) and slope (right). The box represents the 25th to 75th percentile including the line median. The whiskers extend to 1.5 times the interquartile range and the dots are the outliers.

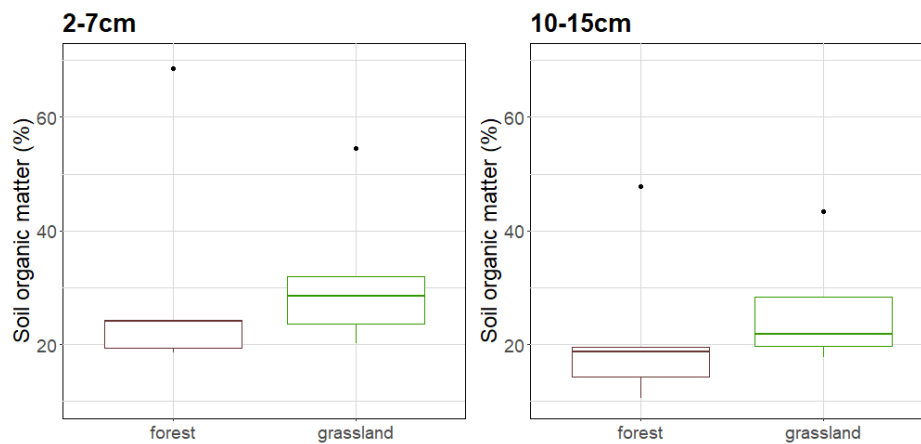


Figure 15: Box plots of the soil organic matter for the forest and grassland sites: 2-7 cm (left) and 10-15 cm (right).

5.2. Soil hydraulic properties

5.2.1. Water retention curves

Figure 16 shows the fitted water retention curves, coloured according to the TWI values. Overall, the moisture content decreased with increasing pF values, but the shape of the curves varied. The water retention curves from 2-7 cm depth showed a nice transition from high TWI soils having more of a S-shaped curve, the curve for sites with a low TWI value being more shaped like an exponential-decrease. The curves of the high TWI sites were flat in the beginning and decreased slowly after about a pF of 1 and showed almost no sign of flattening out at high pF values. The curves of the low TWI steeply decreased initially and then slowly flattened out towards the end. However, moisture content at saturation was similar for sites with a low and high TWI value. Around field capacity, the difference between high and low TWI was most pronounced with higher moisture content in soils with high TWI values. This difference

decreased until approximately the wilting point at a pF of 4.2. After that, differences with TWI values were not as pronounced again.

At a depth of 10-15 cm the transition of the water retention curves from sites with a high to low TWI was not as clear as at 2-7 cm (Figure 16). However, the moisture content at low TWI soils tended to decrease more slowly and more gradually with increasing matric potential than for sites with a high TWI. In addition, soils with high TWI also tended to have higher water retention capacity at low matric potential than soils with lower TWI values.

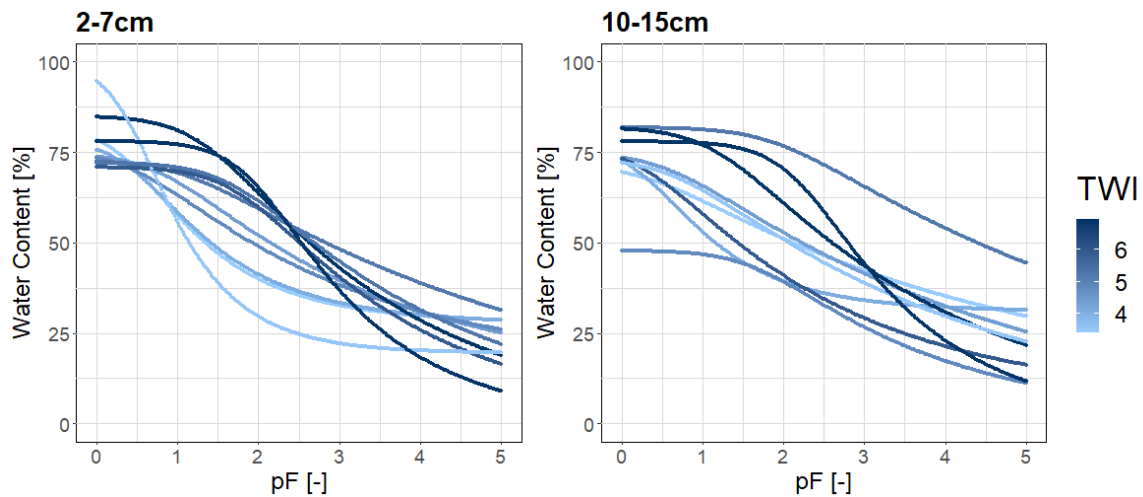


Figure 16: Fitted water retention curves for both soil depths color-coded according to TWI (high TWI: dark blue to low TWI: light blue).

Figure 17 shows the non-fitted water retention curves per site at depths of 2-7 cm and 10-15 cm. This figure also demonstrates that the moisture content decreased with higher pF values at both soil depths at each site. For most sites, the shape of the curve was similar for the two depths. Site 12_1 was very different, with a linear decrease in moisture content with increasing pF at 10-15 cm and an exponential decrease in 2-7 cm. Furthermore, the water retention capacity at both depths was similar for sites 21_2, 21_3, 21_8 and 32_6. At sites 21_1, 21_5 and 21_1, the overall water retention capacity was higher at 10-15 cm than in 2-7 cm, but at sites 21_4 and 21_1 it was lower.

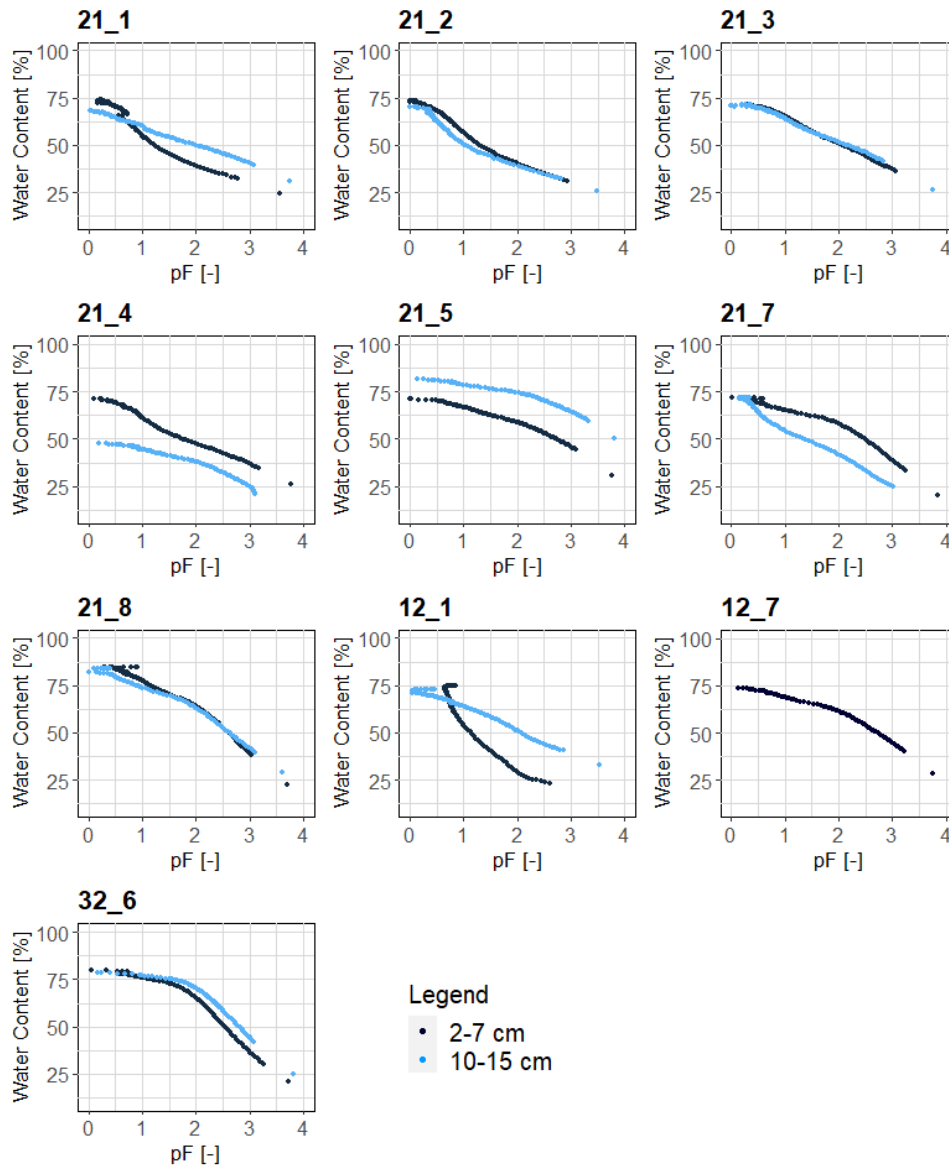


Figure 17: Non-fitted water retention curves for each site for both depths (2-7 cm and 10-15 cm).

Figure 18 compares the moisture content of the soil in depths of 2-7 cm and 10-15 cm at three central pF values: moisture content at saturation (0 pF), field capacity (1.8 pF) and wilting point (4.2 pF). For none of these values, was there a significant difference between the two depths (Table A2). However, this figure shows that as expected the moisture content at saturation was higher than at field capacity, and the moisture content at field capacity was higher than at the wilting point. Furthermore, it highlights that the variance of the moisture content at field capacity was higher than that of the moisture content at saturation (pF=0) or wilting point (pF=4.2).

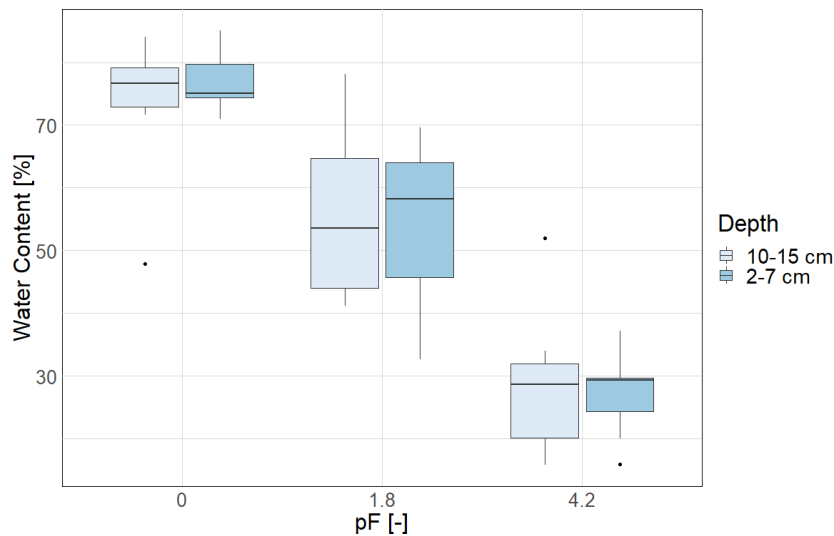


Figure 18: Box plots showing the soil moisture content (water content) at saturation, field capacity ($pF=1.8$), and wilting point ($pF=4.2$) for both depths.

There were some differences between the water retention curves for the forest and grassland soils (Figure 19 and 20). The moisture content at saturation ($pF\ 0$) up to about pF of 3.4 was slightly higher for the grassland soils than the forest soils. At the end of the curve ($pF >4$), the moisture content was higher for the forest soils than grassland soils. The most pronounced difference was observed around field capacity (1.8 pF). The variance of the moisture content of forest soils was more or less the same for all pF values. In contrast, the variance of the moisture content of grassland soils was high around field capacity, low at saturation and low after $pF\ 3$. Figure 19 shows the differences in the shapes of the SWRC between forest and grassland sites. Both grassland and forest sites had S-shaped and exponential-decrease-shaped curves indicating no significant difference between the SWRC shapes of the two vegetation types.

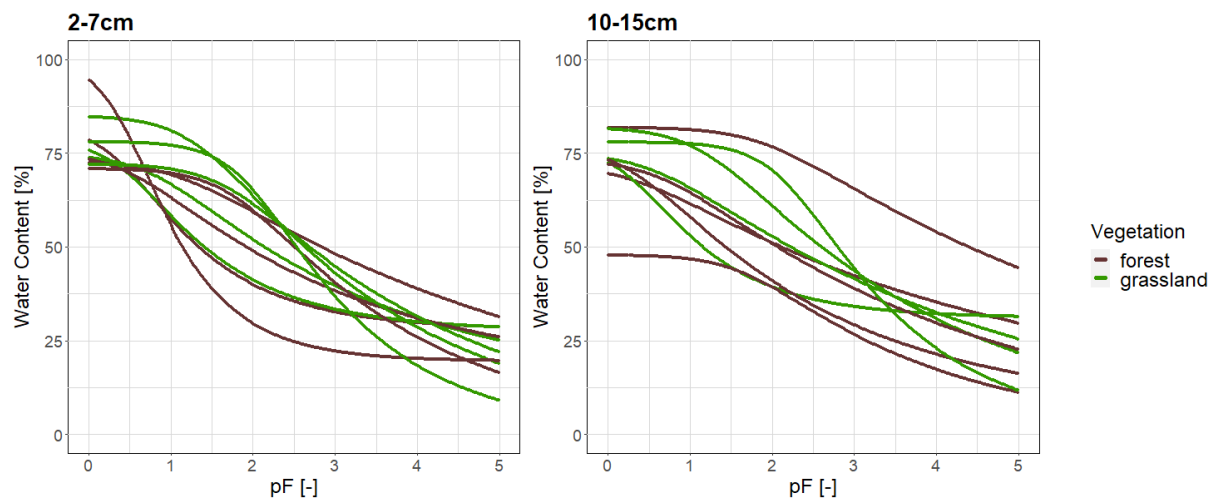


Figure 19: Fitted water retention curves color-coded by vegetation (forest and grassland).

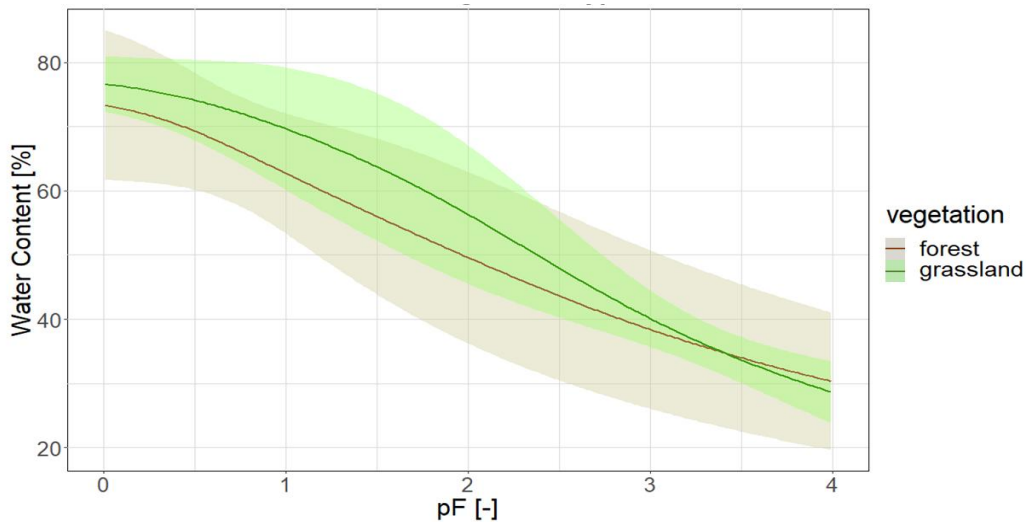


Figure 20: Mean and double standard deviation of fitted water retention curves for forest and grassland sites.

Figure 21 shows the fitting parameter determined by the Van Genuchten equation (and those later used in the HYDRUS-1D model) as a function of the TWI. Alpha was negatively correlated with TWI at 2-7 cm depth, but there was no statistically significant correlation for 10-15 cm depth, nor for n and TWI at either depth (Table A2).

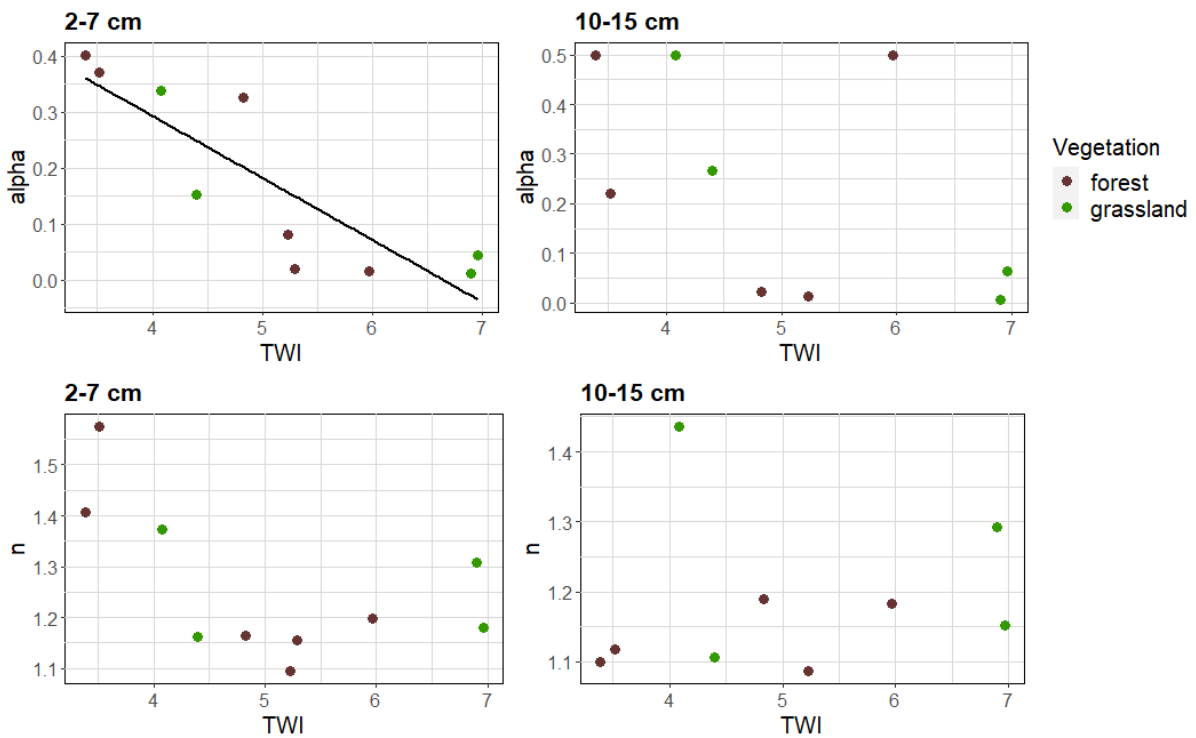


Figure 21: Fitted parameters (n and α) from the Van Genuchten model in relation to topographic wetness index (TWI) for both soil depths. The regression line shows the statistically significant correlation between α and TWI for the 2-7 cm samples.

5.2.2. Drainable porosity

The drainable porosity varied between 7.95 and 42.14 % for the samples taken from 2-7 cm depth and 3.70 and 35.49 % for the samples from 10-15 cm depth. The variance was large for both soil depth, with 10-15 cm samples tending to have values lower than the mean and 2-7 cm samples tending to have values higher than the mean. However, the drainable porosity was not statistically different between the two soil depths (Table A2). There was a negative correlation between drainable porosity and TWI for a depth of 2-7 cm (Figure 22) but for 10-15 cm. There was also no statistically significant relation between the drainable porosity and slope.

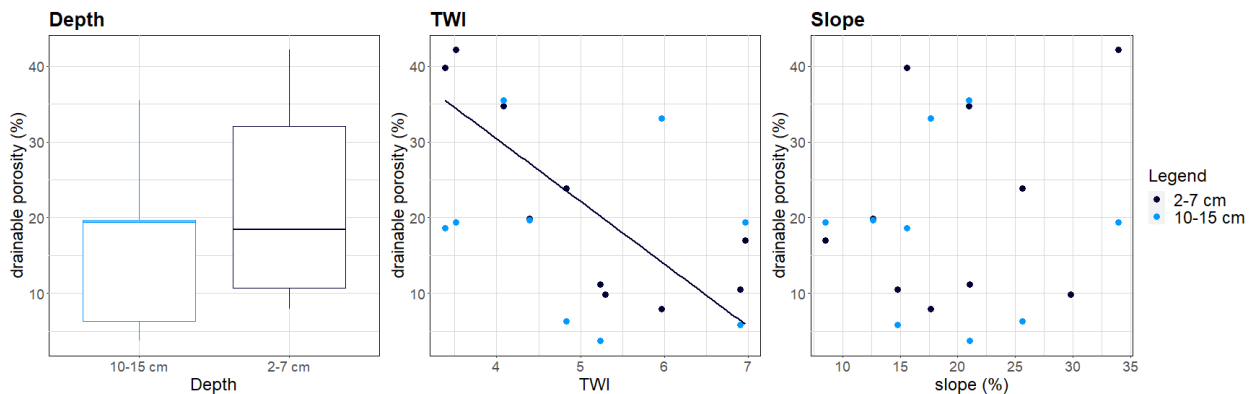


Figure 22: Box plots of the drainable porosity for the two soil depths (left) and the relation between the drainable porosity and TWI (middle), and slope (right). The regression line shows the statistically significant correlation between TWI and drainable porosity at 2-7 cm depth.

5.3. Model simulations

The 1D model did not produce any overland flow for any of the sites. Instead, all water infiltrated into the soil. Figures 23 and 24 show the simulated moisture contents for the 19.08.2022 and 24.06.2022 rainfall events. After both rainfall events, which started at 100 h, the moisture content at 0.5 cm soil depth increased shortly after the event for all forest and grassland sites. Overall, grassland soils at 0.5 cm depth had a higher soil moisture content ranging from about 40% to 80%, while in forest soils it ranged from about 25% to 70%. In the grassland sites, a relation between moisture content and TWI was observed, with soils with low TWI values (light colours) appearing to have lower overall moisture contents than soils with high TWI values. For the sites with high TWI values, the moisture content tended to increase earlier than for soils with low TWI values. Furthermore, the increase in soil moisture was smaller for soils that had already a high moisture content before the rainfall event than for soils with a low moisture content at the start of the simulation.

Comparing both rainfall events, it is visible that the event of 19.08.2022 seemed to lead to a slower and smaller increase in soil moisture and a faster decrease compared to the event of 24.06.2022. The moisture content of the 24.06.2022 event decreased after about 5 hours, while that of the 19.08.2022 event decreased after about 10 hours, which was in line with the longer duration of this event (21 vs 8 hours).

The soil moisture response at 5 cm was similar to those observed at 0.5 cm depth. However, the increase in moisture content started later at 5 cm depth. At a depth of 15 cm, the change in moisture content due to rainfall was less and also starts later than in the shallower soil depths for both rainfall events. Furthermore, changes in moisture content were less pronounced at 15 cm depth during the 24.06.2022 rainfall event than during the 19.08.2022 event. At the 19.08.2022 event, the forest sites all had similar moisture contents, ranging from 60% to about 70%. Soil moisture at 25 cm soil depth only changed for sites with high TWI values. However, there was almost no change in moisture content for the short duration 24.06.2022 event. In addition, changes in matric potential after both rainfall events were small (Figures A4 and A5).

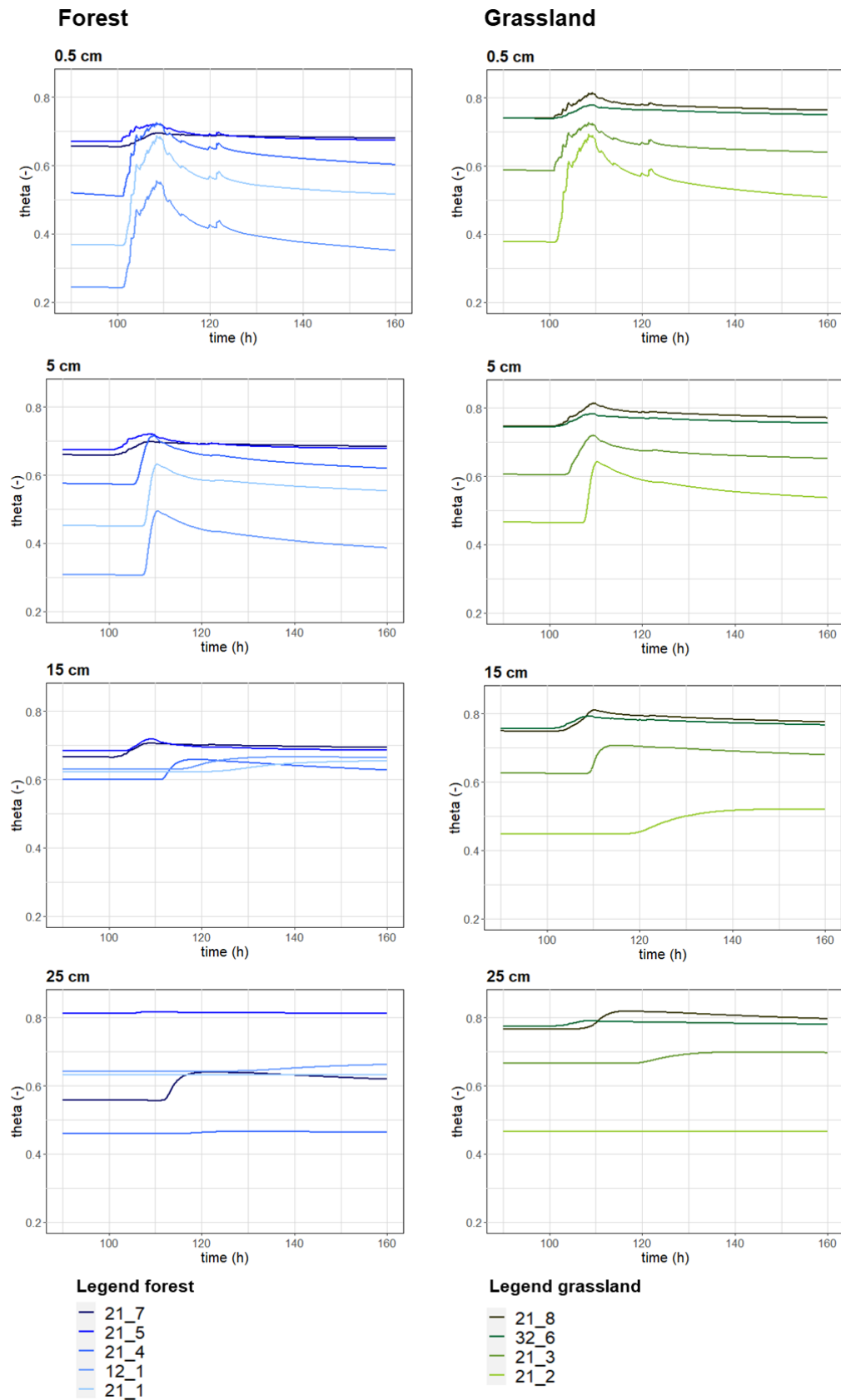


Figure 23: Time series of the simulated soil moisture content during and after the large rainfall event for each forest and grassland site at 0.5 cm, 5 cm, 15 cm and 25 cm below the soil surface. The rainfall event of 19.08.2022 starts at 100 h. The sites are ordered from wet (dark colour) to dry (light colour) based on the topographic wetness index (TWI).

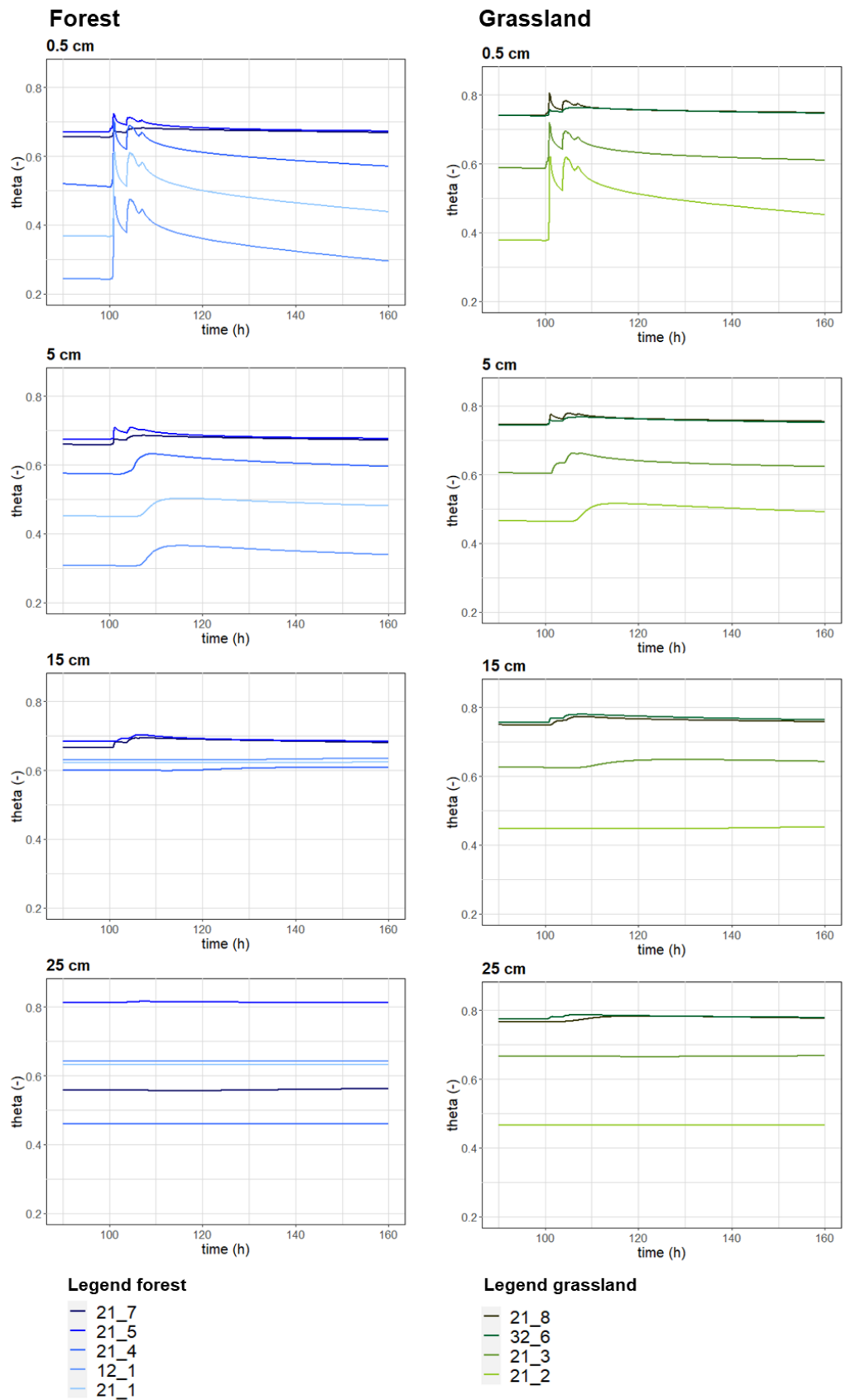


Figure 24: Time series of the simulated soil moisture content for the high-intensity rainfall event for each forest and grassland site at 0.5 cm, 5 cm, 15 cm and 25 cm below the soil surface. The rainfall event of 24.06.2022 starts at 100 h. The sites are ordered from wet (dark colour) to dry (light colour) according to the TWI.

6. Discussion

6.1. Spatial variation of soil hydraulic properties

6.1.1. Soil organic matter

As organic matter depends on topography and slope according to the Catena concept, a correlation between SOM and TWI or slope was expected (cf. Fissore et al., 2017; Fu et al., 2004; Moore et al., 1993; Pachepsky et al., 2001; Pei et al., 2010; Schwanghart and Jarmer, 2011). Although the correlation between SOM and TWI was not significant, there was a trend of increasing SOM with increasing TWI (Figure 14). Higher moisture accumulation in flat areas and depressions and erosion of SOM in steep areas could explain this trend. High moisture content can increase decomposition. However, the Studibach catchment is very wet and at the sites with high moisture contents SOM can be stored due to limited oxygen concentrations and microbial activity. In drier soils (e.g. low TWI) on steeper slopes, the decomposition of SOM is not limited. This effect was also observed in a study by Sierra et al. (2017). Therefore, high SOM contents in soils with high TWI values may have increased the water-holding capacity and decreased the drainable porosity and improved aggregate stability by binding soil particles.

However, the distribution of SOM is influenced by many factors such as vegetation, soil moisture content, soil depth, and others, which interact and influence each other in a complex way. This might be a reason why there was no clear relationship between SOM and TWI. In addition, measurement errors in the laboratory, the small sample size, and many outliers (e.g. 12_1_1 and 21_8_1) could be responsible for the lack of a statistically significant correlation. Furthermore, only one representative sample was taken for each site and depth, which may not accurately represent that site.

6.1.2. Water retention and drainable porosity

In line with the hypothesis, the differences in water retention and drainable porosity were related to the topographic wetness index (Figures 16 and 22). For sites with a high TWI, the soil at 2-7 cm depth has a higher water retention capacity (especially around field capacity) and a larger air entry pressure value than soils at drier locations. Thus, drainable porosity is higher at sites with a low TWI, as also demonstrated by the negative correlation between drainable porosity and TWI for the topsoil layer (2-7 cm).

The effect of topography on the drainable porosity of the topsoil is likely related to the strong influence of macroporosity on water retention. The S-shaped SWRC for sites with a high TWI indicates that it takes longer for the air to enter these soils and that the fraction of micropores is higher for these soils than for soils at sites with a low TWI. The soils at sites with a low TWI are characterized by more macropores, likely due to the activity of soil fauna (e.g. earthworms) and the presence of roots. This indicates that the relation with TWI is at least partly due to the effect of topography on drainage and vegetation. Sites with a low TWI are generally forested and those with a high TWI are grassland sites (Table 2).

The moisture contents between saturation (pF 0) and a pF of about 3.4 were slightly higher for the grassland soils than the forest soils (Figure 20), with the differences in moisture content decreasing with increasing matric potential. This was also demonstrated in the study by Saha et al. (2015) and Pirastru et al. (2013) (see Figure 7). This is reasonable because soil texture is the most important factor at matric potentials that are more negative than field capacity (i.e., higher pF values), which are not influenced by vegetation cover according to Pirastru et al. (2013). The most significant difference in water retention between forest and grassland sites was found around field capacity, with a higher water retention in grassland soils compared to forest soils. This is in agreement with the study by Saha et al. (2015) for soils in north-west India. This may indicate that forest soils are better drained due to the high density of plant roots and soil fauna, which increases porosity and maintains stable macropores, resulting in preferential flow and deep infiltration. Furthermore, this work found a trend towards higher SOM in grassland, which may increase aggregate stability and soil water retention.

However, the results contradict the claims of Dlapa et al. (2020) and Pirastru et al. (2013), who found a lower water retention in grassland soils due to lower soil organic carbon content and a smaller pore space. This suggests that also other factors can influence the water retention of grassland and forest soils. These include the type of forest and grassland cover, whether grassland is used for grazing, and the season in which soil properties are measured. According to several studies, infiltration in grassland soils is higher in summer due to higher microporosity caused by fauna (e.g. earthworm channels), whereas in forest soils porosity is more stable due to more consistent vegetation (Bormann and Klaassen, 2008; Pirastru et al., 2013; Zhou et al., 2008).

Soil compaction may have affected the water retention by altering soil structure. For example, cattle grazing could affect soil structure as compaction reduces pore space, which reduces water holding capacity at low matric potential. Indeed the drainable porosity for the sites in the upper

catchment where there is grazing is lower compared to similar grassland sites in the lower catchments.

Erosion of soil material on steep slopes, and the accumulation in depressions are likely to have a large effect on the water retention as soil texture, which theoretically influences water retention characteristics, does not vary significantly between sites. Thus, although previous studies have found differences in soil textures along a hillslope (Pachepsky et al., 2001; Taye et al., 2018), this was not the case for these study sites. However, measurement errors may have affected the soil texture analysis. Because not all organic matter was removed prior to soil texture analysis, silt and clay content may have been overestimated in the laboratory analysis (cf. Hartmann et al., 2020). This could be a reason for the high clay and silt content, particularly for sample 21_8_2 with high silt values. Samples 21_8_1, 21_8_2, 12_1_1 and 21_7_2 contained much organic material, especially fine roots. In addition, some of the fine soil particles may have been washed out during the saturation of the soil samples.

The relationship between TWI and soil hydraulic properties was not as strong for the deeper soil depth (10-15 cm). This could be due to several reasons, such as the small sample size, measurement errors, and fitting errors. Alternatively, the effect of vegetation cover on soil properties may be less strong for the deeper soil. However, the effect of vegetation on SOM and DP at 2-7 cm and 10-15 cm is similar and shows no significant difference between the two depths (Figure 15 and Figure A3).

6.2. Effect of soil hydraulic properties on hydrological response

6.2.1. Effect of soil hydraulic parameters

Soil hydraulic properties affect infiltration rates and soil moisture responses, and thus potentially also the partitioning of rainfall into infiltration and surface runoff. The observed differences in the soil hydraulic parameters influenced the infiltration rates and soil moisture content, but did not affect the partitioning of rainfall into infiltration and surface runoff, as all rainfall infiltrated into the soil, regardless of the soil hydraulic properties used.

The simulated soil moisture contents varied between the sites, especially in the top 15 cm of the soil (Figures 23 and 24). As conductivity was similar for all grassland or forest sites and only varied with depth, the differences in the soil moisture responses between the sites indicate the influence of the soil water retention parameters and thus the measured SWRC. Because the residual moisture content (wilting point) and the saturated moisture content did not differ

notably for the sites, the influence of these parameter on the simulated soil moisture response is expected to be small. This is supported by the study by Song et al. (2020), who reported a low model sensitivity to changes in the mean residual moisture content. Therefore, the parameters n and α are likely to be the most important influencing factors (cf. Baumhardt et al., 1990).

The parameters n and α are related to the pore size distribution, soil texture, and soil structure, which makes the model results indirectly dependent on these soil properties. As soil texture is not expected to change with vegetation cover (Dlapa et al., 2020; Pirastru et al., 2013) and was not significantly different for the sites of this study, the pore size distribution and soil structure have the largest effects on the simulated soil moisture response. These model parameters reflect the impact of SOM, roots, and soil fauna (see section 6.1.2). More specifically, as parameter α represents the inverse of the air-entry pressure, which depends on the pore space, the maximum pore size is an influencing factor. This factor changes with, for example, soil fauna activity and plant root density, and indirectly influences the simulated model results. The parameter n represents the pore size distribution index and was highly variable across the catchment, but not related to topography (Figure 22).

The differences in the simulated soil moisture are mainly visible for the topsoil (0.5 and 5 cm depth) and are not as pronounced at greater depths. This suggests that the influence of roots, fauna and SOM decreases with depth. Furthermore, the increase in soil moisture content after rainfall events is more delayed and generally smaller with increasing depth because water first infiltrates into the upper layers and needs more time to reach deeper soil depth. The percolation rates also decreased with depth because of the lower saturated conductivity and higher clay content at depth (Table A1). In general, however, water infiltration is limited, which is expected at this research site due to the low permeability of gleysols.

6.2.2. Effect of size and intensity of rainfall

The small differences between the large and high-intensity rainfall event can be explained by the difference in rainfall duration, the total volume of water, and the rainfall intensity. The larger total volume of rainwater and longer duration of the large event, result in a higher moisture contents and deeper infiltration than for the high intensity event. However, infiltration appears to be faster at the beginning of the high-intensity rainfall event due to the higher volume of rainwater in the short period of time. It declines more quickly compared to the large rainfall

event because the rain stops earlier, allowing the water to move downwards (or evaporate) earlier. During the large rainfall event, additional rainwater infiltrates into the soil at the time the rain stops during the high-intensity event.

6.2.3. Model uncertainties and the influence of subsurface lateral flow

The simulated moisture results provide a general but limited understanding of how water is redistributed after a large, intense rainfall event. In contrast to the observations (Feyen et al., 1996; Ragetti et al., 2021; Van Meerveld et al., 2018), surface runoff was not simulated. This lack of simulated surface runoff could be due to several model uncertainties. First, the structure of HYDRUS-1D is a simplification of the natural soil system. As the model is only one-dimensional and only considers vertical flow based on the Richards equation, the model does not consider subsurface lateral flow. In the Studibach catchment, subsurface lateral flow is a significant contributor to surface runoff due to the almost impermeable soil and bedrock. Secondly, more realistic boundary conditions (e.g. changing groundwater levels) could have influenced the model results. However, no such boundary condition was used.

The simulated moisture content suggests that soils at sites with a high TWI have deeper infiltration as the moisture contents in the deeper soil layers is higher for these sites. As reported in previous studies by Franzluebbbers (2002) and Basset et al. (2023), a higher infiltration rate could be due to better soil structure and improved aggregate stability. In flat areas, SOM accumulation is higher, leading to better soil structure, which improves infiltration. In addition, soils with high TWI values have a high moisture content at the start of the simulation, the pores in the top layers of the soil are already filled with water, reducing the capacity for additional infiltration. In the model, water will therefore move downwards into the available pore space, increasing infiltration at deeper soil depths. This is not realistic as in deeper percolation is unlikely for the sites in the Studibach due to the high initial water table and low permeability soils.

7. Conclusions

This thesis shows that the spatial variation of soil hydraulic properties is related to topography. The topographic wetness index was significantly correlated to the drainable porosity, water retention curves, and the variation in soil moisture content and appears to be a good predictor of soil hydraulic properties in the Studibach catchment. Vegetation also influences soil hydraulic properties and infiltration by impacting the density of root channels and soil organic matter content. As soil texture did not vary spatially, soil texture is not expected to have a large influence on water retention characteristics in the catchment. The observed differences in soil hydraulic properties were large enough to affect the distribution of soil moisture throughout the soil profile after large rainfall events. However, they could not explain the observed differences in overland flow and infiltration as the 1D model did not simulate runoff from upslope areas.

In conclusion, this thesis demonstrates the relationship between soil hydraulic properties, infiltration and topography. It also illustrates the need to understand the complex relationship between topography and soil hydraulic properties to understand soil-water processes and interactions between different earth systems. However, the sample size was small, and not all influencing factors could be investigated. Therefore, further research is needed to determine the effect of topography and other environmental factors on the spatial variation of soil hydraulic properties. Furthermore, more realistic 3D model simulations are needed to determine the effect of soil properties and topography on rainfall partitioning at the soil surface.

References

- Abbott, M. B., Bathurst, J. C., Cunge, J. A., O'Connell, P. E., & Rasmussen, J. (1986). An introduction to the European Hydrological System — Systeme Hydrologique Europeen, "SHE", 1: History and philosophy of a physically-based, distributed modelling system. *Journal of Hydrology*, 87(1), 45–59. [https://doi.org/https://doi.org/10.1016/0022-1694\(86\)90114-9](https://doi.org/https://doi.org/10.1016/0022-1694(86)90114-9)
- Agnese, C., Bagarello, V., Baiamonte, G., & Iovino, M. (2011). Comparing Physical Quality of Forest and Pasture Soils in a Sicilian Watershed. *Soil Science Society of America Journal*, 75(5), 1958–1970. <https://doi.org/10.2136/sssaj2011.0044>
- Alaoui, A., Caduff, U., Gerke, H. H., & Weingartner, R. (2011). Preferential Flow Effects on Infiltration and Runoff in Grassland and Forest Soils. *Vadose Zone Journal*, 10(1), 367–377. <https://doi.org/10.2136/vzj2010.0076>
- Ashok K. I., Kishori L. S., Kotha S. R. (2020), Chapter 18 - Hydraulic properties of soil under warming climate, Editor(s): Majeti Narasimha Vara Prasad, Marcin Pietrzykowski, Climate Change and Soil Interactions, *Elsevier*, 473-508. <https://doi.org/10.1016/B978-0-12-818032-7.00018-7>.
- Basset, C., Abou Najm, M., Ghezzehei, T., Hao, X., & Daccache, A. (2023). How does soil structure affect water infiltration? A meta-data systematic review. *Soil and Tillage Research*, 226(September 2022). <https://doi.org/10.1016/j.still.2022.105577>
- Baumhardt, R. L., Römkens, M. J. M., Whisler, F. D., & Parlange, J. -Y. (1990). Modeling infiltration into a sealing soil. *Water Resources Research*, 26(10), 2497–2505. <https://doi.org/10.1029/WR026i010p02497>
- Berhe, A. A., Harden, J. W., Torn, M. S., & Harte, J. (2008). Linking soil organic matter dynamics and erosion-induced terrestrial carbon sequestration at different landform positions. *Journal of Geophysical Research: Biogeosciences*, 113(4), 1–12. <https://doi.org/10.1029/2008JG000751>
- Berhe, A. A., Harden, J. W., Torn, M. S., Kleber, M., Burton, S. D., & Harte, J. (2012). Persistence of soil organic matter in eroding versus depositional landform positions. *Journal of Geophysical Research: Biogeosciences*, 117(2), 1–16. <https://doi.org/10.1029/2011JG001790>
- Beven, K. & Kirkby, M. (1979). A physically based, variable contributing area model of basin hydrology / Un modèle à base physique de zone d'appel variable de l'hydrologie du bassin versant, *Hydrological Sciences Journal*, 24(1), 43-69, <https://doi.org/10.1080/02626667909491834>
- Beven, K. (2012). Rainfall-runoff modelling. *John Wiley & Sons, Ltd.* <https://doi.org/10.1201/9780429423116-33>

- Biswas, A. (2019). Joint multifractal analysis for three variables: Characterizing the effect of topography and soil texture on soil water storage. *Geoderma*, 334(July 2018), 15–23. <https://doi.org/10.1016/j.geoderma.2018.07.035>
- Bormann, H., & Klaassen, K. (2008). Seasonal and land use dependent variability of soil hydraulic and soil hydrological properties of two Northern German soils. *Geoderma*, 145(3–4), 295–302. <https://doi.org/10.1016/j.geoderma.2008.03.017>
- Brunone, B., Ferrante, M., Romano, N., & Santini, A. (2003). Numerical Simulations of One-Dimensional Infiltration into Layered Soils with the Richards Equation Using Different Estimates of the Interlayer Conductivity. *Vadose Zone Journal*, 2(2), 193–200. <https://doi.org/10.2113/2.2.193>
- Celik, I. (2005). Land-use effects on organic matter and physical properties of soil in a southern Mediterranean highland of Turkey. *Soil and Tillage Research*, 83(2), 270–277. <https://doi.org/10.1016/j.still.2004.08.001>
- Corona, C. R., & Ge, S. (2022). Examining subsurface response to an extreme precipitation event using HYDRUS-1D. *Vadose Zone Journal*, (March 2021), 1–15. <https://doi.org/10.1002/vzj2.20189>
- Devi, G. K., Ganasri, B. P., & Dwarakish, G. S. (2015). A Review on Hydrological Models. *Aquatic Procedia*, 4, 1001–1007. <https://doi.org/10.1016/j.aqpro.2015.02.126>
- Dlapa, P., Hrinik, D., Hrabovsky, A., Simkovic, I., Zarnovican, H., Sekucia, F., & Kollar, J. (2020). The Impact of Land-Use on the Hierarchical Pore Size Loamy Soils. *Water*, 12, 339.
- Dougherty, W., Fleming, N. K., Cox, J. W., Chittleborough, D. J., (2004). Phosphorus Transfer in Surface Runoff from Intensive Pasture Systems at Various Scales. *Journal of environmental quality*. 33.
- Dussailant, A. R., Wu, C. H., & Potter, K. W. (2004). Richards Equation Model of a Rain Garden. *Journal of Hydrologic Engineering*, 9(3), 219–225. [https://doi.org/10.1061/\(asce\)1084-0699\(2004\)9:3\(219\)](https://doi.org/10.1061/(asce)1084-0699(2004)9:3(219))
- Dymond, S. F., Bradford, J. B., Bolstad, P. V., Kolka, R. K., Sebestyen, S. D., & DeSutter, T. M. (2017). Topographic, edaphic, and vegetative controls on plant-available water. *Ecohydrology*, 10(8), 1–12. <https://doi.org/10.1002/eco.1897>
- Eijkelkamp (2023). Hand penetrometer Eijkelkamp, URL: <https://www.royaleijkelkamp.com/products/field-measuring-equipment/resistance-to-penetration/mechanical/hand-penetrometer-eijkelkamp-1-m-or-3-m/> (access: 14.07.2023).
- Evrendilek, F., Celik, I., & Kilic, S. (2004). Changes in soil organic carbon and other physical soil properties along adjacent Mediterranean forest, grassland, and cropland ecosystems in Turkey. *Journal of Arid Environments*, 59(4), 743–752. <https://doi.org/10.1016/j.jaridenv.2004.03.002>

- FAO (2015). World reference base for soil resources 2014 - International soil classification system for naming soils and creating legends for soil maps. *Food and Agriculture Organization of the United Nations*, (Vol. 106). <https://doi.org/10.1038/nnano.2009.216>
- Feyen, H., Leuenberger, J., Papritz, A., Gysi, M., Flüher, H., & Schleppei, P. (1996). Runoff processes in catchments with a small scale topography. *Physics and Chemistry of the Earth*, 21(3), 177–181. [https://doi.org/10.1016/S0079-1946\(97\)85581-4](https://doi.org/10.1016/S0079-1946(97)85581-4)
- Fischer, B. M. C., Stähli, M., & Seibert, J. (2017). Pre-event water contributions to runoff events of different magnitude in pre-alpine headwaters. *Hydrology Research*, 48(1), 28–47. <https://doi.org/10.2166/nh.2016.176>
- Fissore, C., Dalzell, B. J., Berhe, A. A., Voegtle, M., Evans, M., & Wu, A. (2017). Influence of topography on soil organic carbon dynamics in a Southern California grassland. *Catena*, 149, 140–149. <https://doi.org/10.1016/j.catena.2016.09.016>
- Foth, H. (1990). Fundamentals of soil science. 15th edition.
- Franzluebbers, A. J. (2002). Water infiltration and soil structure related to organic matter and its stratification with depth. *Soil and Tillage Research*, 66(2), 197–205. [https://doi.org/10.1016/S0167-1987\(02\)00027-2](https://doi.org/10.1016/S0167-1987(02)00027-2)
- Fierer, N., Schimel, J. P., & Holden, P. A. (2003). Variations in microbial community composition through two soil depth profiles. *Soil Biology and Biochemistry*, 35(1), 167–176. [https://doi.org/10.1016/S0038-0717\(02\)00251-1](https://doi.org/10.1016/S0038-0717(02)00251-1)
- Fu, B. J., Liu, S. L., Ma, K. M., & Zhu, Y. G. (2004). Relationships between soil characteristics, topography and plant diversity in a heterogeneous deciduous broad-leaved forest near Beijing, China. *Plant and Soil*, 261(1–2), 47–54. <https://doi.org/10.1023/B:PLSO.0000035567.97093.48>
- Geroy, I. J., Gribb, M. M., Marshall, H. P., Chandler, D. G., Benner, S. G., & Mcnamara, J. P. (2011). Aspect influences on soil water retention and storage. *Hydrological Processes*, 25(25), 3836–3842. <https://doi.org/10.1002/hyp.8281>
- Gonzalez-Sosa, E., Braud, I., Dehotin, J., Lassabatère, L., Angulo-Jaramillo, R., Lagouy, M., ... Michel, K. (2010). Impact of land use on the hydraulic properties of the topsoil in a small French catchment. *Hydrological Processes*, 24(17), 2382–2399. <https://doi.org/10.1002/hyp.7640>
- Green, V. S., Stott, D. E., Norton, L. D., & Graveel, J. G. (2000). Polyacrylamide Molecular Weight and Charge Effects on Infiltration under Simulated Rainfall. *Soil Science Society of America Journal*, 64(5), 1786–1791. <https://doi.org/10.2136/sssaj2000.6451786x>
- Gregory, M. A., Cunningham, B. A., Schmidt, M. F., & Mack, B. W. (1999). Estimating Soil Storage Capacity for Stormwater Modeling Applications. *6th Biennial Stormwater Research and Watershed Management Conference*, 1–14.
- Gutmann, E. D., & Small, E. E. (2005). The effect of soil hydraulic properties vs. soil texture in land surface models. *Geophysical Research Letters*, 32(2), 1–4. <https://doi.org/10.1029/2004GL021843>

- Hartmann, A., Weiler, M., & Blume, T. (2020). The impact of landscape evolution on soil physics: Evolution of soil physical and hydraulic properties along two chronosequences of proglacial moraines. *Earth System Science Data*, *12*(4), 3189–3204. <https://doi.org/10.5194/essd-12-3189-2020>
- Hilberts, A. G. J., Troch, P. A., & Paniconi, C. (2005). Storage-dependent drainable porosity for complex hillslopes. *Water Resources Research*, *41*, 1–13. <https://doi.org/10.1029/2004WR003725>
- Hillel, D. (2003). Introduction to environmental soil physics.
- Islam, Z. (2011). A Review on Physically Based Hydrologic Modeling on Submitted by Zahidul Islam Department of Civil and Environmental Engineering University of Alberta May, 2011. <https://doi.org/10.13140/2.1.4544.5924>
- Jarvis, N., Koestel, J., Messing, I., Moeys, J., & Lindahl, A. (2013). Influence of soil, land use and climatic factors on the hydraulic conductivity of soil. *Hydrology and Earth System Sciences*, *17*(12), 5185–5195. <https://doi.org/10.5194/hess-17-5185-2013>
- Jemai, I., Ben Aissa, N., Ben Guirat, S., Ben-Hammouda, M., & Gallali, T. (2012). On-farm assessment of tillage impact on the vertical distribution of soil organic carbon and structural soil properties in a semiarid region in Tunisia. *Journal of Environmental Management*, *113*, 488–494. <https://doi.org/10.1016/j.jenvman.2012.05.029>
- Kirkham, M. B. (2005). Tensiometers. In *Principles of Soil and Plant Water Relations* (pp. 41–54). <https://doi.org/10.1016/B978-012409751-3/50004-9>
- Kollegger, A.A. (2011). Untersuchung der räumlichen und zeitlichen Verteilung der Bodenfeuchtigkeit am Beispiel des Erlenbaches (Alptal/Schweiz) - Vergleich einer quantitativen und einer qualitativen Messmethode. *Department of Geography, University of Zurich, Zurich*, 1-83.
- Lee, K. E., & Foster, R. C. (1991). Soil fauna and soil structure. *Soil Research*, *29*(6), 745–775. Retrieved from <https://doi.org/10.1071/SR9910745>
- Lin, H. (2010). Earth's Critical Zone and hydrogeology: Concepts, characteristics, and advances. *Hydrology and Earth System Sciences*, *14*(1), 25–45. <https://doi.org/10.5194/hess-14-25-2010>
- Lohse, K. A., & Dietrich, W. E. (2005). Contrasting effects of soil development on hydrological properties and flow paths. *Water Resources Research*, *41*(12), 1–17. <https://doi.org/10.1029/2004WR003403>
- Maskey, S. (2022). Models of unsaturated (vadose) zone. *Catchment Hydrological Modelling*, 59–79. <https://doi.org/10.1016/b978-0-12-818337-3.00007-6>
- Merilä, P., Malmivaara-Lämsä, M., Spetz, P., Stark, S., Vierikko, K., Derome, J., & Fritze, H. (2010). Soil organic matter quality as a link between microbial community structure and vegetation composition along a successional gradient in a boreal forest. *Applied Soil Ecology*, *46*(2), 259–267. <https://doi.org/10.1016/j.apsoil.2010.08.003>

- METER (2021). HYPROP-Fit User Manual. *roup AG Mettlacher Straße 8, 81379 München, Germany*. URL: www.meter-group.com/hyprop-2/#support
- Moore, I. D., Gessler, P. E., Nielsen, G. A., & Peterson, G. A. (1993). Soil Attribute Prediction Using Terrain Analysis. *Soil Science Society of America Journal*, 57(2), 443–452. <https://doi.org/10.2136/sssaj1993.03615995005700020026x>
- Morais, T. G., Teixeira, R. F. M., & Domingos, T. (2019). Detailed global modelling of soil organic carbon in cropland, grassland and forest soils. *PLoS ONE*, 14(9), 1–27. <https://doi.org/10.1371/journal.pone.0222604>
- Mualem, Y. (1976). A New Model for Predicting the Hydraulic Conductivity of Unsaturated Porous Media. *Water Resources Research*, 12(3), 513–522.
- Nyamadzawo, G., Chikowo, R., Nyamugafata, P., & Giller, K. E. (2007). Improved legume tree fallows and tillage effects on structural stability and infiltration rates of a kaolinitic sandy soil from central Zimbabwe. *Soil and Tillage Research*, 96(1–2), 182–194. <https://doi.org/10.1016/j.still.2007.06.008>
- Otoni Filho, T. B., Caetano, A. R., & Otoni, M. V. (2022). In situ Field Capacity in Brazilian Soils and a Derived Irrigation Management Practice Based on Water Suction. *Journal of Agricultural Science*, 14(3), 23. <https://doi.org/10.5539/jas.v14n3p23>
- Pei, T., Qin, C. Z., Zhu, A. X., Yang, L., Luo, M., Li, B., & Zhou, C. (2010). Mapping soil organic matter using the topographic wetness index: A comparative study based on different flow-direction algorithms and kriging methods. *Ecological Indicators*, 10(3), 610–619. <https://doi.org/10.1016/j.ecolind.2009.10.005>
- Pachepsky, Y. A., Timlin, D. J., & Rawls, W. J. (2001). Soil Water Retention as Related to Topographic Variables. *Soil Science Society of America Journal*, 65(6), 1787–1795. <https://doi.org/10.2136/sssaj2001.1787>
- Pali, A. K., Katre, P., & Khalkho, S. (2014). An Unsteady Subsurface Drainage Equation Incorporating Variability of Soil Drainage Properties. *Water Resour Manage*, (28), 2639–2653. <https://doi.org/10.1007/s11269-014-0631-1>
- Pan, T., Hou, S., Liu, Y., & Tan, Q. (2019). Comparison of three models fitting the soil water retention curves in a degraded alpine meadow region. *Scientific Reports*, 9(1), 1–12. <https://doi.org/10.1038/s41598-019-54449-8>
- Pirastu, M., Castellini, M., Giadrossich, F., & Niedda, M. (2013). Comparing the Hydraulic Properties of Forested and Grassed Soils on an Experimental Hillslope in a Mediterranean Environment. *Procedia Environmental Sciences*, 19, 341–350. <https://doi.org/10.1016/j.proenv.2013.06.039>
- Ragettli, S., Tong, X., Zhang, G., Wang, H., Zhang, P., & Stähli, M. (2021). Climate change impacts on summer flood frequencies in two mountainous catchments in China and Switzerland. *Hydrology Research*, 52(1), 4–25. <https://doi.org/10.2166/NH.2019.118>

- Rawls, W. J., & Pachepsky, Y. A. (2002). Using Field Topographic Descriptors To Estimate Soil Water Retention. *Soil Science*, 167(7), 423–435. <https://doi.org/10.1097/01.ss.0000022697.98626.c6>
- Riihimäki, H., Kemppinen, J., Kopecký, M., & Luoto, M. (2021). Topographic wetness index as a Proxy for Soil Moisture: The Importance of Flow-Routing Algorithm and Grid Resolution. *Water Resources Research*, 57(10). <https://doi.org/10.1029/2021WR029871>
- Rinderer, M., Van Meerveld, H. J., & Seibert, J. (2014). Topographic controls on shallow groundwater levels in a steep, prealpine catchment: When are the TWI assumptions valid? *Water Resources Research*, 50(7), 6067–6080. <https://doi.org/10.1002/2013WR015009>
- Romano, N., & Palladino, M. (2002). Prediction of soil water retention using soil physical data and terrain attributes. *Journal of Hydrology*, 265(1–4), 56–75. [https://doi.org/10.1016/S0022-1694\(02\)00094-X](https://doi.org/10.1016/S0022-1694(02)00094-X)
- Schenk, H. J., & Jackson, R. B. (2002). The global biogeography of roots. *Ecological Monographs*, 72(3), 311–328.
- Schwanghart, W., & Jarmer, T. (2011). Linking spatial patterns of soil organic carbon to topography - A case study from south-eastern Spain. *Geomorphology*, 126(1–2), 252–263. <https://doi.org/10.1016/j.geomorph.2010.11.008>
- Selker, J., & Or, D. (2019). Basic Relationships and the Soil Phases Under Equilibrium Conditions. *Soil Hydrology and Biophysics*. <https://doi.org/10.5399/osu/1142>
- Sierra, C. A., Malghani, S., & Loescher, H. W. (2017). Interactions among temperature, moisture, and oxygen concentrations in controlling decomposition rates in a boreal forest soil. *Biogeosciences*, 14(3), 703–710. <https://doi.org/10.5194/bg-14-703-2017>
- Šimůnek, J., M. Šejna, A., Saito, H., Sakai, M., & Genuchten, M. T. Van. (2013). The HYDRUS-1D software package for simulating the movement of water, heat, and multiple solutes in variably saturated media, version 4.17. *HYDRUS Software Series 3D*. Retrieved from https://www.pc-progress.com/Downloads/Pgm_Hydrus1D/HYDRUS1D-4.17.pdf
- Skaggs, R. W., Wells, L. G., & Ghate, S. R. (1978). Predicted and Measured Drainable Porosities for Field Soils. *Biosystems and Agricultural Engineering Faculty Publications*, 21(3), 522–528. <https://doi.org/10.13031/2013.35337>
- Stahr, K., Kandeler, E., Herrmann, L., Streck, T. (2008). *Bodenkunde und Standortlehre*. 10.36198/9783838553450.
- Starr, G. C., Lal, R., Malone, R., Hothem, D., Owens, L., & Kimble, J. (2000). Modeling soil carbon transported by water erosion processes. *Land Degradation and Development*, 11(1), 83–91. [https://doi.org/10.1002/\(SICI\)1099-145X\(200001/02\)11:1<83::AID-LDR370>3.0.CO;2-W](https://doi.org/10.1002/(SICI)1099-145X(200001/02)11:1<83::AID-LDR370>3.0.CO;2-W)

- Stähli, M., Seibert, J., Kirchner, J. W., von Freyberg, J., & van Meerveld, I. (2021). Hydrological trends and the evolution of catchment research in the Alptal valley, central Switzerland. *Hydrological Processes*, 35(4), 1–16. <https://doi.org/10.1002/hyp.14113>
- Stewart, R. D., Rupp, D. E., Najm, M. R. A., & Selker, J. S. (2013). Modeling effect of initial soil moisture on sorptivity and infiltration. *Water Resources Research*, 49(10), 7037–7047. <https://doi.org/10.1002/wrcr.20508>
- BLW, Swisstopo (2012): Digitale Bodeneignungskarte der Schweiz – Wasserdurchlässigkeit, URL: <https://opendata.swiss/de/dataset/digitale-bodeneignungskarte-der-schweiz-wasserdurchlassigkeit> (access: 20.03.2023).
- Taye, M., Simane, B., Selssie, Y. G., Zaitchik, B., & Setegn, S. (2018). Analysis of the spatial variability of soil texture in a tropical highland: The case of the Jema Watershed, Northwestern Highlands of Ethiopia. *International Journal of Environmental Research and Public Health*, 15(9), 1–10. <https://doi.org/10.3390/ijerph15091903>
- Taylor, G. S. (1960). Drainable porosity evaluation from outflow measurements and its use in drawdown equations. *Soil Science*. <https://doi.org/10.1097/00010694-196012000-00004>
- Tromp-van Meerveld, H. J., & McDonnell, J. J. (2006). On the interrelations between topography, soil depth, soil moisture, transpiration rates and species distribution at the hillslope scale. *Advances in Water Resources*, 29(2), 293–310. <https://doi.org/10.1016/j.advwatres.2005.02.016>
- UMS (2015). Manual HYPROP, Version 2015-01, UMS GmbH, Gmunder Straße 37, Munich, Germany. 1-96. URL: www.metergroup.com/hyprop-2/#support
- USDA (2017). Soil Survey Manual. *Agriculture Handbook*, 18, 1-669. <https://doi.org/10.2307/1233734>
- Van Dam, J. C., & Feddes, R. A. (2000). Numerical simulation of infiltration, evaporation and shallow groundwater levels with the Richards equation. *Journal of Hydrology*, 233(1), 72–85.
- Van Genuchten, M. Th. (1980). A closed-form equation for predicting the hydraulic conductivity of unsaturated soils. *Soil Science Society of America Journal*, 44, 892–898. Retrieved from [https://hwbddocuments.env.nm.gov/Los Alamos National Labs/TA 54/11569.pdf](https://hwbddocuments.env.nm.gov/Los%20Alamos%20National%20Labs/TA54/11569.pdf)
- Van Meerveld, I., H. J., Fischer, B. M. C., Rinderer, M., Stähli, M., & Seibert, J. (2018). Runoff generation in a pre-alpine catchment: A discussion between a tracer and a shallow groundwater hydrologist. *Geographical Research Letters*, 44(2), 429–452. <https://doi.org/10.18172/cig.3349>
- Van Meerveld, I., Kirchner, J. W., Vis, M. J. P., Assendelft, R. S., & Seibert, J. (2019). Expansion and contraction of the flowing stream network alter hillslope flowpath lengths and the shape of the travel time distribution. *Hydrology and Earth System Sciences*, 23, 4825–4834. <https://doi.org/10.5194/hess-23-4825-2019>

- Ventrella, D., Castellini, M., Di Prima, S., Garofalo, P., & Lassabatère, L. (2019). Assessment of the Physically-Based Hydrus-1D Model for Simulating the Water Fluxes of a Mediterranean Cropping System. *Water*, *11*(1657), 1–19. <https://doi.org/10.3390/w11081657>
- Wang, X., Cammeraat, L. H., Wang, Z., Zhou, J., Govers, G., & Kalbitz, K. (2013). Stability of organic matter in soils of the belgian loess belt upon erosion and deposition. *European Journal of Soil Science*, *64*(2), 219–228. <https://doi.org/10.1111/ejss.12018>
- Wang, C., Zhao, C. Y., Xu, Z. L., Wang, Y., & Peng, H. H. (2013). Effect of vegetation on soil water retention and storage in a semi-arid alpine forest catchment. *Journal of Arid Land*, *5*(2), 207–219. <https://doi.org/10.1007/s40333-013-0151-5>
- Weil, R., & Brady, N. (2017). *The Nature and Properties of Soils*. 15th edition.
- Weiler, M., & McDonnell, J. (2004). Virtual experiments: A new approach for improving process conceptualization in hillslope hydrology. *Journal of Hydrology*, *285*(1–4), 3–18. [https://doi.org/10.1016/S0022-1694\(03\)00271-3](https://doi.org/10.1016/S0022-1694(03)00271-3)
- Winzeler, H. E., Owens, P. R., Read, Q. D., Libohova, Z., Ashworth, A., & Sauer, T. (2022). Topographic wetness index as a Proxy for Soil Moisture in a Hillslope Catena: Flow Algorithms and Map Generalization. *Land*, *11*(11). <https://doi.org/10.3390/land11112018>
- Zhou, X., Lin, H. S., & White, E. A. (2008). Surface soil hydraulic properties in four soil series under different land uses and their temporal changes. *Catena*, *73*(2), 180–188. <https://doi.org/10.1016/j.catena.2007.09.009>

Appendix

Table A1: HYDRUS-1D model parameters for water flow.

Site	Soil depth (cm)	Qr (-)	Qs (-)	alpha (1/cm)	n (-)	Ksat (cm/h)	l (-)
21_1	0 – 10	0.295	0.822	0.4021	1.407	19.111	0.50
	10 – 40	0.340	0.717	0.5	1.1	9.656	0.50
	40 – 50	0.068	0.380	0.008	1.090	0.200	0.50
21_2	0 – 15	0.296	0.785	0.3389	1.373	11.663	0.50
	15 – 30	0.319	0.766	0.5	1.436	5.932	0.50
	30 – 50	0.068	0.380	0.008	1.090	0.200	0.50
21_3	0 – 17	0.296	0.747	0.1537	1.163	11.663	0.50
	17 – 32	0.309	0.750	0.2673	1.106	5.932	0.50
	32 – 50	0.068	0.380	0.008	1.090	0.200	0.50
21_4	0 – 20	0.298	0.754	0.325	1.165	19.111	0.50
	20 – 40	0.158	0.479	0.0215	1.19	9.656	0.50
	40 – 50	0.068	0.380	0.008	1.090	0.200	0.50
21_5	0 – 20	0.372	0.728	0.0819	1.094	19.111	0.50
	20 – 40	0.519	0.819	0.0128	1.086	9.656	0.50
	40 – 50	0.068	0.380	0.008	1.090	0.200	0.50
21_7	0 – 18	0.236	0.709	0.0166	1.197	19.111	0.50
	18 – 35	0.201	0.771	0.5	1.183	9.656	0.50
	35 – 40	0.068	0.380	0.008	1.090	0.200	0.50
21_8	0 – 15	0.263	0.850	0.0438	1.18	11.663	0.50
	15 – 30	0.287	0.841	0.0639	1.152	5.932	0.50
	30 – 50	0.068	0.380	0.008	1.090	0.200	0.50
12_1	0 – 10	0.200	0.748	0.3698	1.575	19.111	0.50
	10 – 33	0.281	0.729	0.2198	1.118	9.656	0.50
	33 – 50	0.068	0.380	0.008	1.090	0.200	0.50
32_6	0 – 15	0.159	0.801	0.0111	1.307	11.663	0.50
	15 – 30	0.200	0.791	0.00647	1.293	5.932	0.50
	30 – 50	0.068	0.380	0.008	1.090	0.200	0.50

Table A2: List of statistical tests and p-values.

variables	depth (cm)	statistical test	p-value	statistical significance
bulk density and depth		Mann–Whitney U test	0.2526	no
clay and TWI	2-7	Spearman’s rank correlation	0.0831	no
clay and TWI	10-15	Spearman’s rank correlation	0.1710	no
clay and TWI	both	Spearman’s rank correlation	0.0188	yes
SOM and depth		Mann–Whitney U test	0.1128	no
SOM and vegetation	2-7	Mann–Whitney U test	0.5476	no
SOM and vegetation	10-15	Mann–Whitney U test	0.4127	no
SOM and vegetation	both	Mann–Whitney U test	0.2775	no
SOM and TWI	2-7	Spearman’s rank correlation	0.9186	no
SOM and TWI	10-15	Spearman’s rank correlation	0.0857	no
SOM and TWI	both	Spearman’s rank correlation	0.2216	no
SOM and slope	2-7	Spearman’s rank correlation	0.7588	no
SOM and slope	10-15	Spearman’s rank correlation	0.3853	no
SOM and slope	both	Spearman’s rank correlation	0.3651	no
DP and depth		Mann–Whitney U test	0.4377	no
DP and TWI	2-7	Spearman’s rank correlation	0.0068	yes
DP and TWI	10-15	Spearman’s rank correlation	0.5890	no
DP and TWI	both	Spearman’s rank correlation	0.0123	yes
DP and slope	2-7	Spearman’s rank correlation	0.6320	no
DP and slope	10-15	Spearman’s rank correlation	0.6989	no
DP and slope	both	Spearman’s rank correlation	0.8635	no
alpha and TWI	2-7	Spearman’s rank correlation	0.0005	yes
alpha and TWI	10-15	Spearman’s rank correlation	0.1313	no
n and TWI	2-7	Spearman’s rank correlation	0.2042	no
n and TWI	10-15	Spearman’s rank correlation	0.4933	no
moisture content and depth (pF 1.8)		Mann–Whitney U test	0.9682	no
moisture content and depth (pF 4.2)		Mann–Whitney U test	0.7802	no
moisture content and depth (pF max)		Mann–Whitney U test	0.9682	no

Table A3: Precipitation of large rainfall event of 19.08.2022 in 10-minute intervals.

time (s)	P (mm/10min)	time (s)	P (mm/10min)	time (s)	P (mm/10min)
00:00:00	0.1	07:30:00	4.2	15:20:00	0
00:10:00	0.9	07:40:00	2.7	15:30:00	0
00:20:00	0.6	07:50:00	2.5	15:40:00	0
00:30:00	0.6	08:00:00	2.8	15:50:00	0
00:40:00	0.2	08:10:00	2.2	16:00:00	0
00:50:00	0.6	08:20:00	3.1	16:10:00	0
01:00:00	0.6	08:30:00	2	16:20:00	0
01:10:00	0.4	08:40:00	1.9	16:30:00	0
01:20:00	0.4	08:50:00	2.2	16:40:00	0
01:30:00	0.2	09:00:00	0.9	16:50:00	0
01:40:00	0.6	09:10:00	0.2	17:00:00	0
01:50:00	1.6	09:20:00	0.4	17:10:00	0
02:00:00	2.2	09:30:00	0.4	17:20:00	0
02:10:00	0.5	09:40:00	0.2	17:30:00	0
02:20:00	0.7	09:50:00	0.4	17:40:00	0
02:30:00	0.6	10:00:00	0.6	17:50:00	0
02:40:00	1.3	10:10:00	1	18:00:00	0
02:50:00	2.1	10:20:00	0.7	18:10:00	0
03:00:00	2.9	10:30:00	0.6	18:20:00	0
03:10:00	2.7	10:40:00	0.3	18:30:00	0
03:20:00	1.3	10:50:00	0.3	18:40:00	0.2
03:30:00	1	11:00:00	0.2	18:50:00	0.5
03:40:00	1	11:10:00	0.1	19:00:00	0.2
03:50:00	0.7	11:20:00	0.2	19:10:00	0
04:00:00	1.3	11:30:00	0.1	19:20:00	0
04:10:00	1.7	11:40:00	0.1	19:30:00	0
04:20:00	1	11:50:00	0.1	19:40:00	0.1
04:30:00	1.3	12:00:00	0.1	19:50:00	0
04:40:00	1.4	12:10:00	0	20:00:00	0
04:50:00	1.4	12:20:00	0	20:10:00	0.1
05:00:00	1.9	12:30:00	0	20:20:00	0.1
05:10:00	2.3	12:40:00	0	20:30:00	1.2
05:20:00	1.9	12:50:00	0.5	20:40:00	0.2
05:30:00	2.4	13:00:00	0.2	20:50:00	0.6
05:40:00	1.1	13:10:00	0.2	21:00:00	0.4
05:50:00	1.8	13:20:00	0.2	21:10:00	0.1
06:00:00	2.2	13:30:00	0.1	21:00:00	0.4
06:10:00	2.2	13:40:00	0.1	21:10:00	0.1
06:20:00	2.6	13:50:00	0.1		
06:30:00	2.3	14:00:00	0		
06:40:00	2.9	14:10:00	0		
06:50:00	2.6	14:20:00	0		
07:00:00	1.7	14:30:00	0		
07:10:00	3.1	14:40:00	0		
07:20:00	2.2	14:50:00	0.1		

Table A4: Precipitation of high-intensity rainfall event of 24.06.2022 in 10-minute intervals.

time (s)	P (mm/10min)	time (s)	P (mm/10min)	time (s)	P (mm/10min)
00:00:00	0.1	02:50:00	0	05:40:00	0.2
00:10:00	0.3	03:00:00	0	05:50:00	0
00:20:00	0.9	03:10:00	0	06:00:00	0.1
00:30:00	0.2	03:20:00	0	06:10:00	0.1
00:40:00	0.7	03:30:00	0	06:20:00	0.1
00:50:00	1.6	03:40:00	0	06:30:00	0.6
01:00:00	10.5	03:50:00	2.7	06:40:00	0.3
01:10:00	3.6	04:00:00	2.8	06:50:00	0.7
01:20:00	0.4	04:10:00	1.7	07:00:00	0.7
01:30:00	0	04:20:00	2.2	07:10:00	0.4
01:40:00	0	04:30:00	1.4	07:20:00	0.2
01:50:00	0	04:40:00	1.3	07:30:00	0.1
02:00:00	0	04:50:00	0.7	07:40:00	0
02:10:00	0	05:00:00	1.1	07:50:00	0
02:20:00	0	05:10:00	0.7	08:00:00	0
02:30:00	0	05:20:00	0.5	08:10:00	0.1
02:40:00	0	05:30:00	0.4		

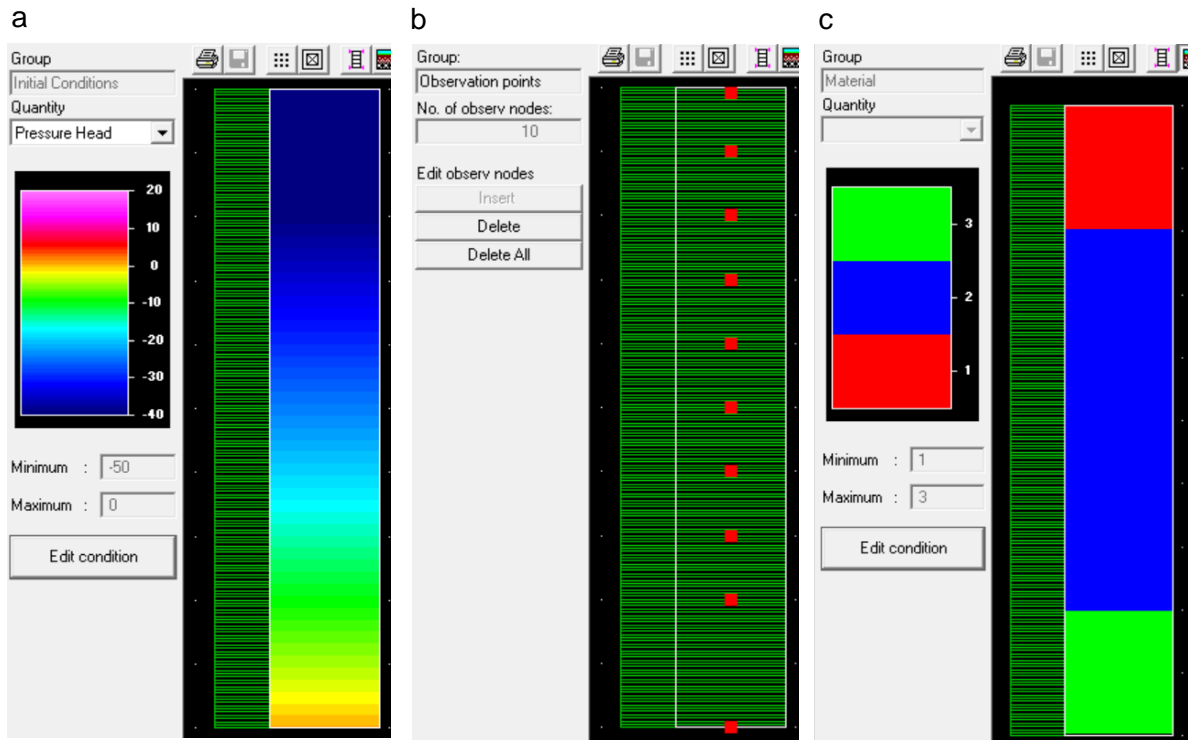


Figure A1: HYDRUS-1D screenshots of the initial pressure head condition (a), location of 10 observation nodes for which the soil moisture data were plotted (b) and an example of the location of the different soil layers (site 21_1) (c).

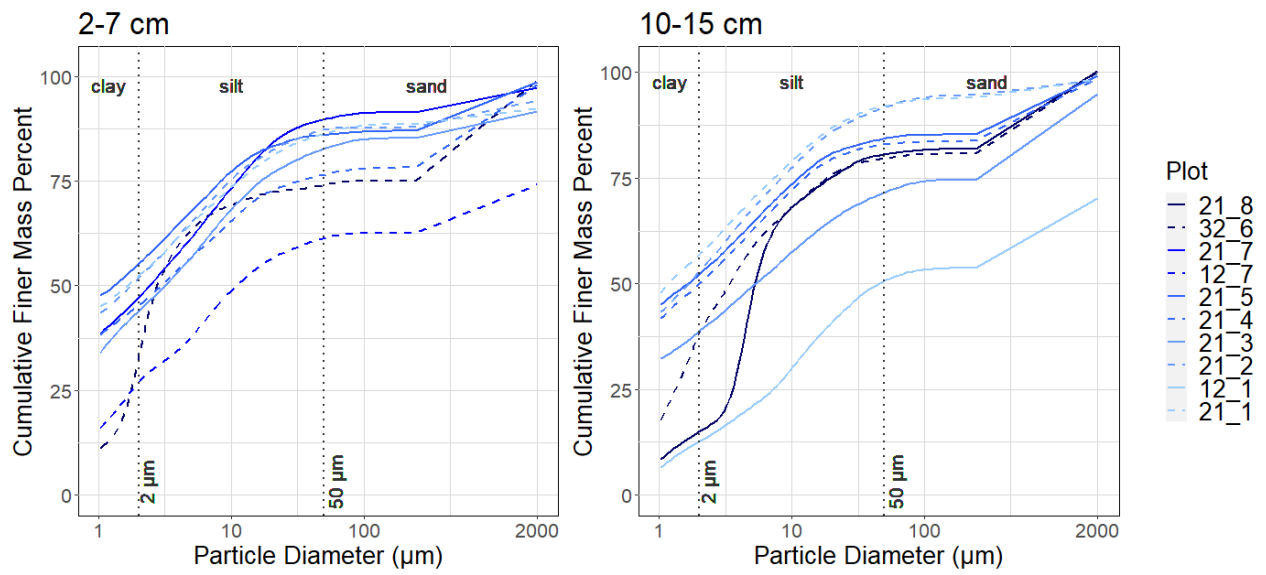


Figure A2: Grain size distribution for the collected samples. Note that the sites in the legend are ordered from wet (dark colour) to dry (light colour) based on TWI.

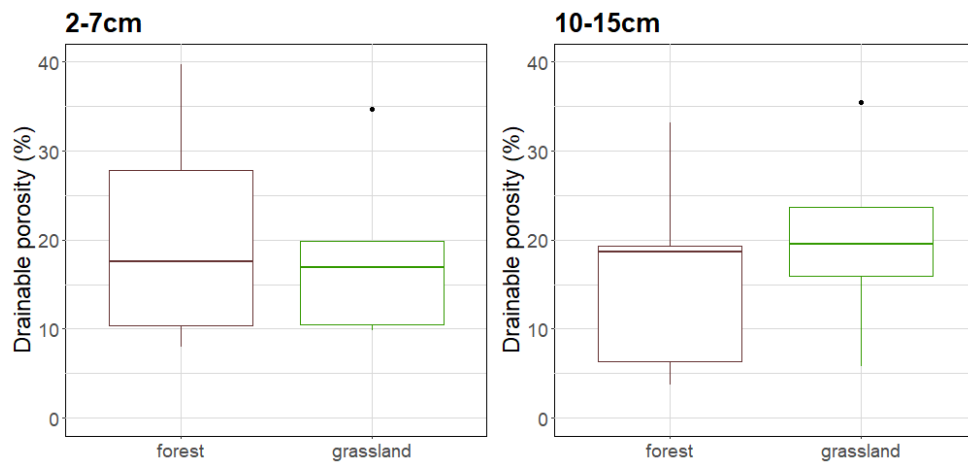


Figure A3: Box plots of the drainable porosity for the forest and grassland sites: 2-7 cm (left) and 10-15 cm (right).

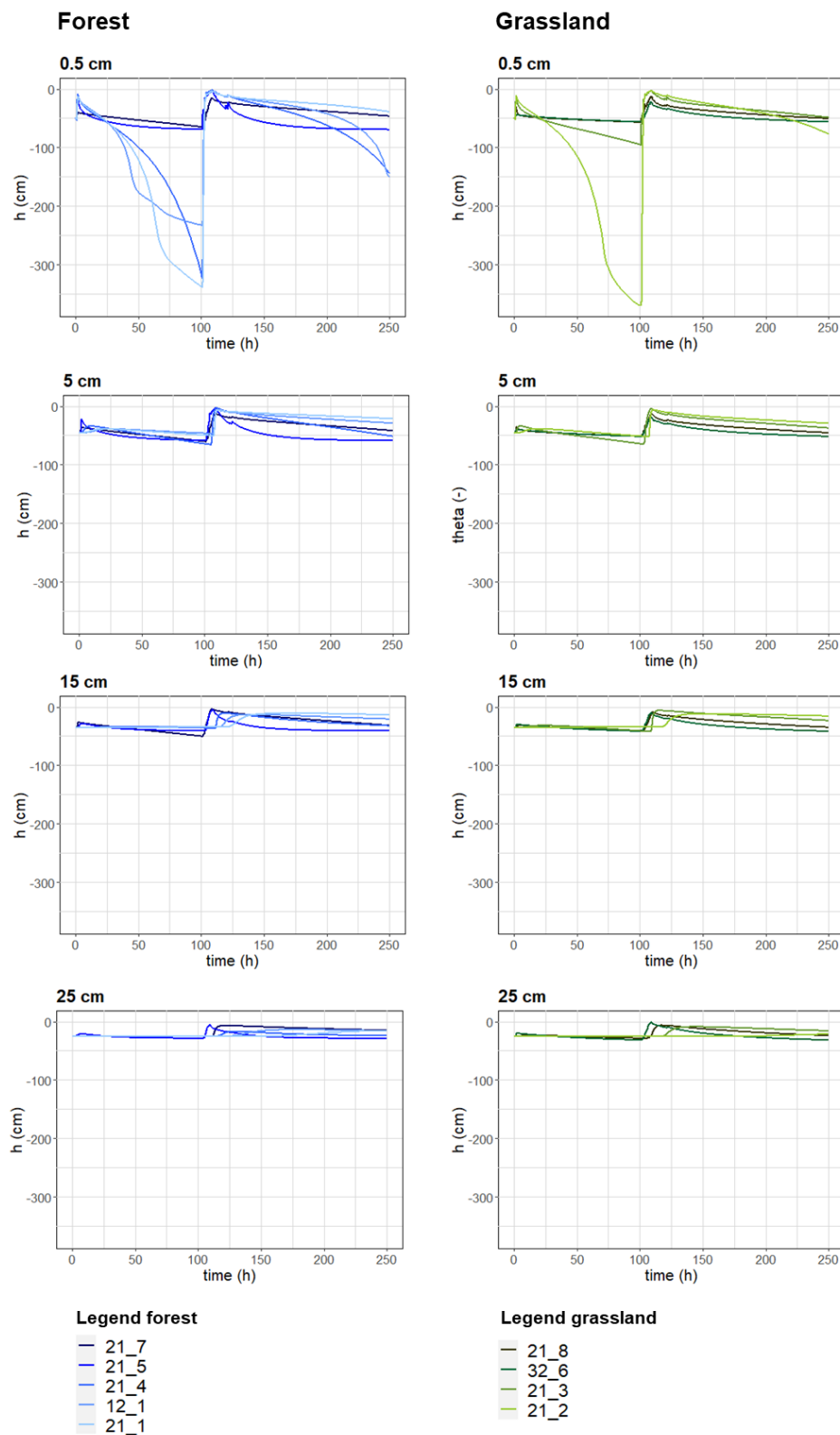


Figure A4: Simulated pressure head at 0.5 cm, 5 cm, 15 cm and 25 cm below the soil surface during the large rainfall event for each forest and grassland site. The large rainfall event of 19.08.2022 starts at 100 h. The sites are ordered in the legend from wet (dark colour) to dry (light colour) according to the topographic wetness index (TWI).

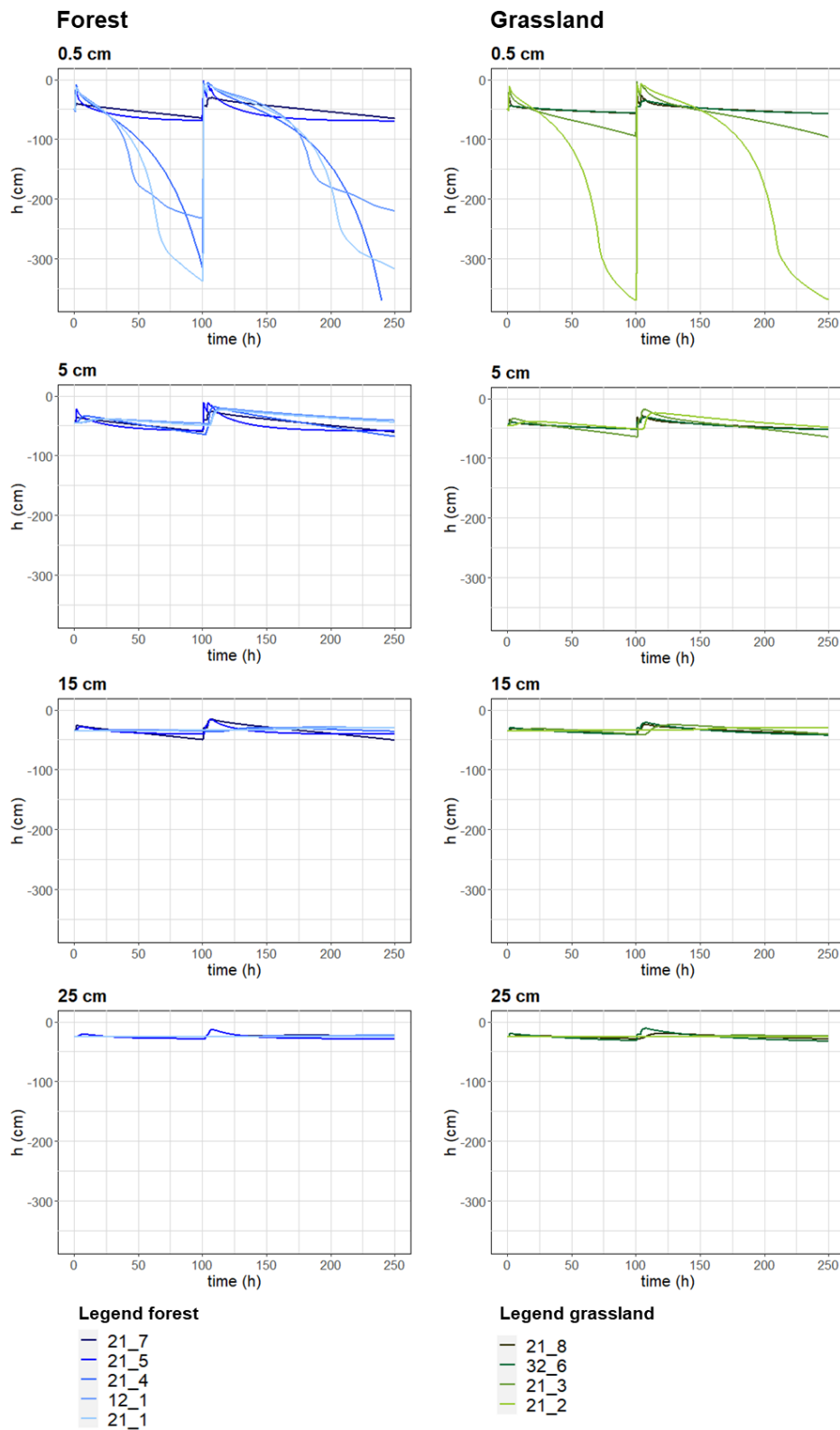


Figure A5: Simulated pressure head at 0.5 cm, 5 cm, 15 cm and 25 cm below the soil surface during the high-intensity rainfall event for each forest and grassland site. The measured rainfall event of 24.06.2022 starts at 100 h. The sites are ordered from wet (dark colour) to dry (light colour) according to the topographic wetness index (TWI).

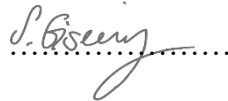
Personal declaration

I hereby declare that the submitted Thesis is the result of my own, independent work. All external sources are explicitly acknowledged in the Thesis.

Name

Sonja Eisenring

Signature

A handwritten signature in cursive script, appearing to read 'S. Eisenring', written over a dotted line.

Date

26.09.2023